Ocean Sci., 22, 2027–2058, 2026
https://doi.org/10.5194/os-22-2027-2026

Ocean Science

The past evolution of marine heatwaves and their drivers in the southern North Sea

Tobias Schulzki[1], **Franziska U. Schwarzkopf**[1], **and Arne Biastoch**[1,2]

[1]GEOMAR Helmholtz Center for Ocean Research, Kiel, Germany
[2]Christian-Albrechts Universität zu Kiel, Kiel, Germany

Correspondence: Tobias Schulzki (tschulzki@geomar.de)

Received: 5 March 2026 – Discussion started: 11 March 2026
Revised: 1 June 2026 – Accepted: 15 June 2026 – Published: 30 June 2026

Abstract. Marine heatwaves (MHWs) are defined as prolonged periods of anomalously high ocean temperatures. These events can have severe impacts on marine ecosystems and, if they occur at the surface, can feed back on the atmosphere, changing inland air temperatures and precipitation.

We use a comprehensive set of model, reanalysis, and observational datasets to investigate recent changes in North Sea MHWs. All datasets show a significant warming trend, accompanied by a marked increase in the frequency of MHWs. In contrast, the maximum intensity of MHWs has decreased in many regions of the North Sea, including the German Bight. If the linear trend in temperature is removed, only a few MHWs have been detected after 2019, suggesting natural variability has damped the effect of the long-term warming.

While distinct weather patterns are associated with the onset of MHWs, their occurrence alone is not sufficient to trigger them. As the heat content is an integrated quantity, the ocean temperature at the beginning of the season (ocean preconditioning) is a key factor, in addition to prevailing weather patterns during the season. As a consequence, only in winter we find a significant dependency of MHWs on established climate indices. In our study region, MHWs result from a combination of short-term weather-related variability and longer-term seasonal to decadal variability.

Furthermore, we find that the evolution of the surface temperature in the German Bight is largely determined by local atmospheric conditions rather than remote variability in the Atlantic. Although the inflow of warm water through the English Channel is important, it is the atmosphere that controls its volume transport and temperature. Whether the atmospheric conditions themselves are linked to remote variability in the Atlantic Ocean remains to be studied.

1 Introduction

The North Sea, located on the Northwest European Shelf, has been warming at a rate of 0.4 °C per decade over the last 40-years (Mohamed et al., 2025) and therefore about twice as fast as the globally averaged sea surface temperature (SST). Along with this long-term warming the frequency and duration of extreme temperature events, known as marine heatwaves (MHWs), have increased in recent decades (Mohamed et al., 2025; Chen and Staneva, 2024).

Marine heatwaves are defined as prolonged periods of anomalously high ocean temperature (Hobday et al., 2016) and have been linked to devastating impacts on marine ecosystems all over the world oceans. This includes for example coral bleaching and the loss of seagrass or kelp forest (Smale et al., 2019; Smith et al., 2023). A prominent example comes from western Australia where a MHW in 2011 led to changes in ecosystem composition (Wernberg et al., 2013) and a major loss of seagrass (Arias-Ortiz et al., 2018). In the Mediterranean Sea the exceptional 2003 MHW was linked to mass mortality of at least 25 benthic macro-invertebrate species (Garrabou et al., 2009).

In the North Sea, Mohamed et al. (2025) suggest MHWs to have an effect on the chlorophyll-a concentration. Semmouri et al. (2023) find MHWs to be the most likely cause for an abundance decrease of copepods in the southern North Sea and Deschamps et al. (2024) argue that MHWs have seasonally dependent impacts on mesozooplankton in the central German Bight. Therefore, MHWs may affect the fundamental components of the food web, but further research is needed to fully understand their impact on North Sea ecosystems and to establish a clear link between individual MHWs and major ecosystem changes.

MHWs can affect ecosystems, but when they occur at the surface, they also feed back on the atmospheric circulation. Coastal MHWs were found to often coincide with warmer, moister and more stagnant air in coastal regions, which is associated with higher thermal discomfort in urban areas (Hu, 2021; Okajima et al., 2025). A warmer ocean surface leads to more evaporation and a reduced land-sea temperature difference during the day. These effects led to stronger convective precipitation and a further warming of the UK's inland temperature during the 2023 MHW in the western North Sea (Berthou et al., 2024).

As one of the world's most important fishing grounds an increase in strength, duration and/or frequency of MHWs in the North Sea could have widespread impacts. Especially the coast of the German Bight in the southeastern North Sea, that is the focus of our research, supports millions of residents and hosts critical infrastructure and economic activity. Therefore, understanding secondary impacts on the coasts, including potential feedbacks on the atmospheric circulation for example, is essential.

Most of the knowledge on MHWs in the North Sea stems from satellite-based observations (Chen and Staneva, 2024; Jacobs et al., 2024; Mohamed et al., 2025, 2023; Lin et al., 2025). At the surface, satellite-based datasets are often considered to provide a ground truth, but it was noted by Zhang et al. (2024) that commonly used datasets can yield significantly different results. This applies to both the mean characteristics of extreme events and long-term trends, highlighting the need to better understand the robustness of the MHWs evolution across datasets.

Furthermore, satellite datasets only provide information about the near-surface ocean, but even in the shallow parts of the North Sea, surface values may not reflect anomalies in the entire water column (Mathis et al., 2015). Berthou et al. (2024) for example find anomalies during the 2023 MHW to peak in a very thin surface layer of a few meters depth, with considerably lower temperature anomalies below. Detailed knowledge of the depth structure of MHWs, however, is very important for the expected biological impacts (e.g. Garrabou et al., 2009). For a comprehensive understanding of the drivers and four-dimensional characteristics of MHWs, other variables than just the surface temperature provided by satellites are needed. Models forced by observed atmospheric conditions and ocean reanalysis can provide physically consistent ocean-atmosphere states during MHWs. This includes for example three-dimensional ocean currents and air-sea heat fluxes. Because ocean reanalysis products incorporate satellite observations, their SST is expected to closely match observations. Forced models that do not incorporate ocean observations are more suited to study the heat budget of the ocean, because, in contrast to reanalysis, they do not contain any artificial sources/sinks of heat. A downside is that they more easily develop biases. For both, forced models and reanalysis, the vertical temperature profile strongly depends on the model set-up (for example mixing parameterizations, vertical resolution and tidal mixing). A systematic comparison of MHWs in different satellite, reanalysis and forced model datasets has not been performed for the North Sea, but is of major importance for a more detailed study of MHW drivers and impacts.

While summer MHWs gained most attention and are overall well understood, MHWs in other seasons could have markedly different drivers. For example high-pressure systems with clear skies and weak winds over the North Sea that have been linked to summer MHWs (Berthou et al., 2024; Mohamed et al., 2025) are expected to cause a cooling of the near-surface ocean rather than a warming in winter. Previous studies have linked the occurrence of MHWs in the North Sea to different climate indices that represent such weather patterns. Lin et al. (2025) find winter MHWs to be influenced by the states of the North Atlantic Oscillation (NAO) and East Atlantic Pattern (EAP). In summer they find MHWs characteristics to change with the NAO or El Niño Southern Oscillation Index (ENSO), dependent on the state of the Atlantic Multidecadal Variability (AMV). On interannual to decadal timescales Mohamed et al. (2025, 2023) only find a dependency of MHW characteristics on the AMV and EAP indices. However, except for the AMV, climate indices reflect specific weather patterns that are more likely related to the heat fluxes than the absolute temperature. Given the fact that the temperature is determined by the integrated effect of the heat fluxes, a strong heat flux anomaly causes a strong temperature change, but not necessarily a high absolute temperature. Therefore, specific weather patterns (e.g. an NAO type pattern) may only trigger MHWs, if they persist long enough or if they occur when the North Sea is already warm.

In addition to the atmospheric conditions, the ocean itself plays an important role for the temperature variability in the North Sea. The North Sea is characterised by a mean cyclonic flow that is fed by an inflow of warm water across the northern boundary (between Scotland and Norway) and through the English Channel. Although the volume transport through the English Channel is much smaller compared to the northern inflow, it was found to be important for the temperature variability and development of MHWs in the southern North Sea, including the German Bight, due to its high temperature (Chen et al., 2021; Mathis et al., 2015; Lin et al., 2025). In comparison to the atmosphere, the ocean circulation varies on longer timescales and may provide long-term predictability of MHW statistics. Changes in the ocean circulation were for example shown to allow for skillful predictions of interannual MHW statistics in the North Atlantic and possibly also in the North Sea (Hövel et al., 2022). Apart from the circulation, the local stratification was found to be important for the development and characteristics of MHWs (Berthou et al., 2024). In very shallow parts of the German Bight, the water column is permanently mixed due to effects of winds and tides, but the more offshore regions can be intermittently stratified (van Leeuwen et al., 2015). Chen et al. (2022) suggest MHWs themselves to be responsible for intermittent stratification in these areas. The interaction of oceanic and atmospheric variability on different timescales from days (individual weather patterns) over seasons (e.g. positive NAO winter) to years and decades (e.g. low frequency circulation changes) have not been investigated, but are necessary to establish causal links between climate indices and the occurrence of MHWs.

Given the lack of a systematic comparison of North Sea MHWs across various datasets and a lack of fundamental knowledge about the processes causing variability in their characteristics, we aim to address the following questions:

- How robust are the characteristics of MHWs in the North Sea in different observation and model-based datasets?
- How and why have the characteristics of MHWs changed over the past 40 years?
- How does variability on different timescales interact to generate MHWs?
- What is the influence of remote variability in the Atlantic on MHWs in the North Sea?

We focus on the southern North Sea, especially the German Bight, but also examine MHWs across the basin to place recent changes in a broader context. After assessing the recent evolution of MHWs in multiple datasets, we analyze output of a forced ocean model to study the drivers of MHWs and relationships between individual MHWs and variability on longer timescales. Finally, we explore how remote variability in the Atlantic Ocean influences the North Sea's temperature.

2 Data

For a robust assessment of MHWs in the North Sea we utilize different datasets spanning the entire range from hindcast models, over ocean reanalysis to interpolated satellite products. In general, the main advantage of models is the continuous availability of data in space and time. Additionally, they provide physically consistent ocean and atmosphere states during MHWs. At the same time, they are usually subject to biases and may not resolve all important processes. Satellite datasets are provided with different levels of processing. Level 4 datasets also provide continuous data in space and time, but they involve complicated steps to fill gaps that are often associated with many choices and uncertainties. The less processing (e.g. level 3 datasets), the more data is missing in space and/or time, which prevents directly applying the MHW detection that requires at least 30-years of daily data at a single grid point. An overview of the datasets used is provided in Table 1.

2.1 VIKING20X – global hindcast

VIKING20X (short: V20) is a global ocean general circulation model configuration based on the NEMO code (version 3.6; Madec, 2016) at 1/4° horizontal resolution with an embedded 1/20° nest in the Atlantic (Biastoch et al., 2021). This translates into a grid spacing of about 3 km in the North Sea. The nest domain includes the entire North Sea and large parts of the Baltic Sea. On both grids, 46 z-levels are used. The grid cell thickness increases from 6 m at the surface to 250 m in the deep ocean. The model configuration has been successfully used to study MHWs on the Canadian Shelf (Großelindemann et al., 2022) and throughout the entire Atlantic (Schulzki et al., 2025).

The experiment analysed here (VIKING20X.L46-KTS001; Schulzki et al., 2026a) follows the experimental design recommended by the OMIP-II protocol for the first model cycle (Tsujino et al., 2020). Accordingly, the experiment is initialized from rest and temperature and salinity from the World Ocean Atlas 2013 climatology (Locarnini et al., 2013; Zweng et al., 2013). The surface heat and momentum fluxes are derived from reanalyzed atmospheric states provided by the JRA55-do v1.4 dataset (Tsujino et al., 2018) using bulk formulae. The namelist settings follow the “VIKING20X-JRA-OMIP” experiment described in Biastoch et al. (2021) with a few differences that were applied to further improve the representation of the North Sea in the model. The most important differences are a new bathymetry with a more realistic coastline in the nest domain (in particular in the North Sea) and a different distribution of runoff. In VIKING20X.L46-KTS001, runoff is not only added to the uppermost grid cell, but more realistically distributed over the water column. The depth range over which the runoff is distributed depends on the climatological strength of the runoff (Madec, 2016) and is about 12 m for rivers entering the North Sea. For rivers outside the North Sea it can be up to 50 m. Additionally, the surface air pressure is used as a forcing and directly impacts the dynamics of the ocean. The simulations based on VIKING20X do not include tidal forcing. The comparison of different datasets described below, as well as additional experiments with and without tides in a model with lower horizontal resolution (not shown), suggest only a small impact of tides on the characteristics of surface MHWs in our focus region (German Bight).

To study the sensitivity of the North Sea to remote temperature variability in the Atlantic we conducted a 10-year long sensitivity experiment (VIKING20X.L46-KTS002). In this experiment the heat flux inside and outside the North Sea are derived from different decades. The experiment branches off from the reference experiment (VIKING20X.L46-KTS001) in 2010. Within the North Sea, heat and momentum fluxes are derived from the atmospheric state of the years 2010 to 2019. Therefore, the atmospheric state in the sensitivity and reference experiments are exactly the same, but the heat and mo-

Table 1. Overview of datasets used in this study. The horizontal resolution refers to approximate values for the German Bight and the vertical resolution is valid for the uppermost model grid cell.

Short name	type	horizontal resolution	vertical resolution	years	ocean data assimilation
V20	forced (global) model	3 km	6 m	1958–2023	–
BSH	forced (regional) model	0.9 km	2 m	2016–2023	–
CST1	forced (regional) model	5 km	5 m	1948–2007	–
G12	(global) ocean reanalysis	9 km	1 m	1993–2023	SST, SSH, T & S profiles
NWS	(regional) ocean reanalysis	7.5 km	1 m	1993–2023	SST, SSH, T & S profiles
OST	L4 satellite product	5 km	–	1982–2023	–
OIS	L4 satellite product	20 km	–	1982–2023	–
DMI	L4 satellite product	2 km	–	1982–2023	–

mentum fluxes may differ as they depend on the ocean state. Outside the North Sea, the momentum flux is derived from the same period (2010–2019), but the surface heat flux is derived from the atmospheric state starting in 1990 and ending 1999. The experiment is compared to the years 2010–2019 in the reference experiment. This allows us to isolate the effect of changing ocean temperature outside the North Sea, while maintaining atmospheric conditions inside the North Sea, including the wind driven transport across the North Sea's boundary.

2.2 BSH model – regional hindcast

Although VIKING20X is a highly capable model for simulating the large-scale Atlantic circulation, it was not optimised for simulating the dynamics of marginal seas. To compare our results with a forced model that was specifically designed to simulate the North Sea circulation, we use output from the HIROMB-BOOS-Model (HBM) based operational model of the Federal Maritime and Hydrographic Agency (BSH; Brüning et al., 2014). The data (short name: BSH) was obtained from https://data.bsh.de/OpenData/OperationalModel/ (last access: 10 January 2025). This regional model has a horizontal resolution of 0.9 km in the German Bight and 5 km in the remaining North Sea. The model uses 24 vertical levels of 2–5 m thickness. The grid cell thickness is fixed, but their centre with respect to a fixed depth axis varies temporally with sea surface height. The temperature is provided after interpolation onto such a fixed depth axis. Additionally the value of the uppermost model level was used without interpolation as the "surface" temperature. The model is forced by operational forecasts provided by the German Weather Service (DWD). Due to the use of tidal forcing at the open boundaries of the regional model and a higher horizontal and vertical resolution, which is also connected to a more realistic bathymetry, the BSH model is expected to simulate the physical conditions in the German Bight more realistically than VIKING20X. However, the model data is only available after 2016. Therefore, no MHW statistics (that are based on a 30-year baseline) can be derived from this dataset and it was only used to validate the vertical structure of MHW events that occurred after 2016.

2.3 CoastDat 1 – regional hindcast

Similar to the BSH model the coastDat1 dataset (short: CST1) was created with a focus on the North Sea, including tides. The data was obtained from the World Data Center for Climate (https://doi.org/10.1594/WDCC/coastDat-1_HAMSOM, HZG, 2012). It is based on the HAMburg Shelf Ocean Model (HAMSOM) with a 20 by 20 km horizontal resolution and 19 vertical levels with a vertical resolution of 5 m at the surface (Meyer et al., 2011). Thus the horizontal resolution is lower compared to VIKING20X and the BSH model. The vertical resolution is similar to VIKING20X, but lower compared to the BSH model. HAMSOM is a regional model of the North Sea and lateral boundary boundary conditions were obtained from a coarse-grid model of the Northwest-European Shelf Sea. The model was forced by 6-hourly NCEP/NCAR reanalysis fields. The available data ranges from 1948 to 2007. Only the common time period compared with the other datasets (1980–2007) is used here.

2.4 GLORYS12v1 – global ocean reanalysis

In contrast to the previous three model configurations that only incorporate atmospheric observations (via atmospheric reanalysis or initialized forecasts), the GLORYS12 version 1 reanalysis (short G12) additionally assimilates ocean observations (Lellouche et al., 2021). In particular, this includes SST from satellites. The data was obtained from the E.U. Copernicus Marine Service (https://doi.org/10.48670/moi-00021, E.U. Copernicus Marine Service Information (CMEMS), 2024d). GLORYS12 is a NEMO-based model with a global 1/12° resolution (about 9 km in the North Sea) and 50 vertical levels. The vertical spacing is 1 m at the surface and increases with depth (22 levels are within the first 100 m). In addition to satellite-based SST measurements, GLORYS12 also assimilates temperature and salinity profiles from the Argo database. GLORYS12 uses a reduced-order Kalman filter approach for small-scale corrections towards observations and a 3D variational (3D-Var) approach to correct larger scales (Lellouche et al., 2021). These approaches have major advantages compared to a simple nudging for example, but they can still introduce spurious sources of heat. The atmospheric forcing is provided by the ECMWF ERA-Interim reanalysis. As VIKING20X, GLORYS12 does not include tidal forcing (although the assimilation of observations implicitly introduces the effect of tides in GLORYS12, especially close to the surface). The dataset covers the years from 1993 to 2023.

2.5 European Northwest Shelf Reanalysis – regional ocean reanalysis

Similar to the comparison between VIKING20X and the BSH model, the GLORYS12 reanalysis is a global model and was not designed with the North Sea in focus. The European Northwest Shelf reanalysis (short: NWS) on the other hand was specifically set-up to simulate the dynamics of the Northwest European Shelf. The data was obtained from the E.U. Copernicus Marine Service (https://doi.org/10.48670/moi-00059, E.U. Copernicus Marine Service Information (CMEMS), 2024a). It is based on the NEMO ocean model and assimilates observations, including SST from satellite measurements and vertical temperature profiles from various data sources. In contrast to GLORYS12, only a variational assimilation scheme, NEMOvar (Waters et al., 2015), is used. The atmospheric forcing is provided by the ECMWF ERA5 atmospheric reanalysis. In contrast to the previous model set-ups that use z-levels in the vertical, the NWS reanalysis uses 51 hybrid s-sigma terrain-following coordinates. The data is provided after interpolation onto a regular grid with 24 depth levels. The surface value is not interpolated and based on a layer of less than 1 m thickness. Furthermore, the model incorporates tidal forcing at the open boundaries and the equilibrium tide from a tidal model. The dataset covers the years from 1993 to 2023.

2.6 OSTIA – L4 satellite observations

A dataset that does not involve a numerical model is the OSTIA (short: OST) product created by the UK MetOffice (Good et al., 2020). Data was obtained from https://doi.org/10.48670/moi-00168 (E.U. Copernicus Marine Service Information (CMEMS), 2024c) (1982–2021) and https://doi.org/10.48670/moi-00165 (E.U. Copernicus Marine Service Information (CMEMS), 2025) (2022–2023). OSTIA provides processing level 4 satellite observations. It uses SST derived from Advanced High Resolution Radiometer (AVHRR) and microwave radiometer measurements. In addition to satellite measurements, in-situ temperature observations from buoys, for example, are used. The different data sources are blended using the NEMOvar scheme. Although NEMOvar is often used together with the NEMO ocean model (e.g. NWS), this dataset does not involve the numerical ocean model step and is therefore distinct from the ocean reanalysis datasets. The dataset is provided on a $1/20°$ regular grid (about 5 km in the North Sea) and covers the years from 1982 to 2023.

2.7 NOAA OISST – L4 satellite observations

Similarly, the NOAA OISST version 2.1 (short: OIS) uses satellite based AVHRR measurements together with in-situ measurements from various platforms, including ships and Argo floats (Huang et al., 2021). Data was obtained from https://www.ncei.noaa.gov/data/sea-surface-temperature-optimum-interpolation/v2.1/access/avhrr/ (last access: 30 October 2024). In contrast to OSTIA, an optimal interpolation scheme is used to create a gap-free dataset instead of the NEMOvar scheme. The data is provided on a regular $1/4°$ grid (about 20 km in the North Sea) and covers the years from 1982 to 2023.

2.8 DMIOI – L4 satellite observations

Another level 4 processing dataset is provided by the Danish Meteorological Institute based on the DMIOI system (Høyer and She, 2007; Høyer and Karagali, 2016). The data was obtained from https://doi.org/10.48670/moi-00156, E.U. Copernicus Marine Service Information (CMEMS), 2024b. The DMI dataset (short: DMI) is based on satellite observations from different infrared and microwave sensors and interpolated using an optimal interpolation scheme. Key differences to the previously mentioned datasets are that no additional in-situ data is used and the very high horizontal resolution of the dataset ($1/50°$ or about 2 km in the North Sea). The dataset covers the years from 1982 to 2023.

3 Methods

3.1 Definition of marine heatwaves

Marine heatwaves are defined following the definition of Hobday et al. (2016). For each day of the year, the climatological mean and 90th percentile of all temperature values within an 11 d window are estimated. The climatology and 90th percentile are then smoothed using a 31 d moving average. A MHW is present if the temperature exceeds the seasonally varying 90th percentile for at least five consecutive days. If the gap between two MHWs does not exceed 2 d, they are considered a single event. This definition was applied separately to all grid points of the datasets.

While the Hobday et al. (2016) definition is accepted by almost all researchers in the MHW community, various baselines to define the "normal" temperature are used. In this study, we apply two of the most commonly used baselines.

First we apply a fixed baseline, where the climatology is calculated for a 30-year period that is common to all datasets (1993–2022). Second, we use a detrended baseline where the linear trend (calculated based on the full overlap period 1993–2023) was subtracted from the temperature timeseries before performing the MHW detection. The choice of the baseline changes the interpretation of the results and depends on the research question (Amaya et al., 2023). The fixed baseline maintains the impact of multi-decadal trends, but it is removed using the detrended baseline (see for example Schulzki et al., 2025). How this affects the detected MHWs is discussed in more detail in later sections of this study. We have also tested to account for seasonal variations in the trend, as suggested by Smith et al. (2025), by removing a trend that depends on the day of year. Since the trend (at least in the German Bight) does not show a clear seasonal cycle, the following results are not sensitive to the exact procedure that is used to remove the trend.

Definition of regional MHW events

To study the seasonality, drivers and depth structure of MHWs it is important to transition from MHW detected at individual grid points to MHW "events". Events are considered to have a certain spatial extent and a well-defined start and end date. There are different possibilities to achieve this. Here regional MHW events are defined based on the mean temperature of a specific subdomain of the North Sea. In this study we focus on the German Bight in the southeastern North Sea (see Fig. 2). The MHW detection is then applied to the mean temperature timeseries for the German Bight. This ensures that a significant part of the region is in a MHW state, when a MHW event is detected. A downside of this method is that potentially strong MHWs in parts of the subdomain could be masked by anomalously cold temperatures in another part. However, the typical extent of MHWs in the North Sea is larger than the German Bight region and therefore usually the entire German Bight region is in a MHW state at the same time. In contrast to other choices, e.g. a clustering and tracking of MHW "features" in space and time, or a threshold for the number of grid points in MHW state, the chosen method requires the least arbitrary choices and is not sensitive to the grid resolution. The latter is particularly important, as we aim to compare various datasets provided on different grids.

To ensure that only MHWs are analysed that have occurred in the real ocean with high certainty, we define validated events. A MHW simulated by VIKING20X is considered validated, if at least two of the satellite-based datasets show at least one MHW day during the modelled MHW event. This allows for MHWs to be validated if their start/end date does not perfectly match the satellite observations, but overlapping MHWs exist in multiple datasets.

3.2 Budget for MHW events and composites

To identify the main drivers of MHWs in the German Bight and link them to specific patterns of atmospheric variability we calculate a heat budget for the German Bight region.

The budget is calculated for the uppermost model layer, which is directly related to the SST. In particular in summer, not the entire water column is well mixed during MHWs even in the shallow German Bight. A budget for the entire mixed layer is not advantageous here because VIKING20X does not accurately resolve the mixed layer depth in very shallow regions such as the southern North Sea. This is related to the definition of the mixed layer (e.g. density change relative to a fixed depth) and the relatively coarse vertical resolution. The heat content change associated with a MHW is calculated as the difference in ocean heat content between the minimum within 5 d prior to the MHW onset and the maximum within 5 d after the onset. This ensures that individual MHWs are well separated and that we investigate the weather-related variability that leads to MHWs on timescales of days. Because several local temperature maxima may be reached during one MHW event (that can be caused by different drivers) we focus on the initial onset (first crossing of the temperature threshold) here.

The heat content OHC is calculated from:

$$\mathrm{OHC} = \rho_0 c_p \int\limits_A T \, \mathrm{d}A \Delta z \tag{1}$$

Here A is the area of the region for which the budget is calculated (e.g. North Sea or German Bight) and T the temperature. Δz is vertical extent of the surface layer and $\rho_0 = 1026\,\mathrm{kg\,m^{-3}}$ and $c_p = 3991.87\,\mathrm{J\,kg^{-1}\,°C^{-1}}$ are the reference density and specific heat capacity. The values are taken from the NEMO routine that is used to calculate the surface heat flux. The ocean heat transport is split into a term related to temperature advection ($\mathrm{OHT_{adv}}$) and another related to volume change ($\mathrm{OHT_{vol}}$). This is achieved by introducing a time dependent domain-averaged reference temperature T_{ref} as suggested by Lee et al. (2004) and Zhang et al. (2018):

$$\begin{aligned} \mathrm{OHT} =& \rho_0 c_p \int\limits_L u_\perp T \, \mathrm{d}L \Delta z \\ =& \rho_0 c_p \int\limits_L u_\perp (T - T_{\mathrm{ref}}) \, \mathrm{d}A \Delta z \\ &+ \rho_0 c_p T_{\mathrm{ref}} \int\limits_L u_\perp \, \mathrm{d}A \Delta z \\ =& \mathrm{OHT_{adv}} - \mathrm{OHT_{vol}} \end{aligned} \tag{2}$$

$u_\perp$ is the velocity normal to a section L. $\mathrm{OHT_{adv}}$ is zero if the temperature advected is the same as the domain-average temperature, while $\mathrm{OHT_{vol}}$ represents changes in volume transport only. In a closed domain, the divergence of $\mathrm{OHT_{vol}}$

($\nabla \cdot \mathrm{OHT}_{\mathrm{vol}}$) is proportional to the horizontal volume transport divergence. In the Boussinesq NEMO model it cancels out with the corresponding vertical term based on the continuity equation. Therefore, the heat budget can be formulated as:

$$\begin{aligned}\frac{\mathrm{dOHC}}{\mathrm{d}t} &= \nabla \cdot \mathrm{OHT}_{\mathrm{adv}} + \mathrm{HFX} + \mathrm{VHT}_{\mathrm{adv}} + \mathrm{Mixing} \\ &= \nabla \cdot \mathrm{OHT}_{\mathrm{adv}} + \mathrm{HFX} + \mathrm{Res} \qquad (3)\end{aligned}$$

HFX is the surface heat flux and $\mathrm{VHT}_{\mathrm{adv}}$ the advective part of the vertical heat transport into the surface layer. The surface heat flux is calculated and stored by the NEMO ocean model. This heat content change is then decomposed into the contribution of vertical and horizontal processes. The vertical processes (mixing and $\mathrm{VHT}_{\mathrm{adv}}$) are summarized in a single term, named the residual here.

We also calculate the heat budget for the entire German Bight from the surface to the bottom using the same method. In this case Δz is replaced by the integral over all vertical levels. When integrated over the whole water column, vertical redistributions of heat do not change the heat content and the residual term becomes zero (except for a negligible contribution from horizontal diffusion across the domain boundaries).

3.2.1 Definition of MHW drivers

To identify the main drivers of MHWs we calculate the contribution of the different heat budget terms to the change in ocean heat content during the onset of MHWs.

The heat flux contribution is calculated from the difference between the surface heat flux and heat lost to deeper model levels (i.e. the net gain of heat caused by the surface heat flux). The latter mainly results from turbulent mixing caused by unstable stratification or winds. In the model this mixing is parameterized by the Turbulent Kinetic Energy (TKE) scheme (Biastoch et al., 2021; Blanke and Delecluse, 1993). Tides could also drive mixing, but were found to be less important in sensitivity experiments (not shown). Note that we assume that the difference between surface heat flux and vertical exchange represents the net effect of the heat flux on the surface model level. This assumption is justified, because a large ocean heat transport is linked to strong winds, such that the entire southern North Sea is well mixed to the bottom. Otherwise, a depth dependency of the heat transport could lead to vertical exchange of heat without any contribution from the surface heat flux. The ocean heat content contribution is calculated from the heat transport across the lateral boundaries of the German Bight as explained above. The heat flux and heat transport contributions add up to 100 %, that is, their sum explains the entire heat content change associated with the development of a MHW. One of the terms may be larger than 100 %, if the other component contributes negatively (i.e. damps the heat gain).

We define heat transport-driven MHWs as all MHWs where the ocean heat transport contributes more than 50 % to the heat gain during the MHW onset. Note however that the heat flux can still contribute to these events. If the surface heat flux (net vertical) contribution is larger than 50 % we also calculate the contribution of the individual heat flux components (long wave: LW, short wave: SW, sensible: SE and latent LA) to the total heat flux. As several components often contribute similarly to a single event, we consider all heat flux components that contribute at least 30 % to be the main drivers. The value was chosen here, because for few MHWs, 3 of the components contributed almost equally ($1/3 \approx 30\,\%$). Although this is still a subjective choice, the chosen value is only relevant for events in which multiple components contribute similarly, but events where a dominant driver can be identified are not affected. Furthermore, this method is advantageous, because it does not require an assumption about the number of heat flux components that contribute to an event. This could be misleading, as a weather pattern related to strong SW and SE anomalies for example could be distinct from one that leads to a strong SW anomaly only.

For all events, we calculate the oceanic and atmospheric conditions during the onset phase by taking the mean over the same period that is used to calculate the contributions (see above). The resulting fields and vertical temperature profiles for each event are then used for composites of all events attributed to the respective main drivers.

3.2.2 Heat transport decomposition

In order to study the contribution of temperature and circulation changes to the total ocean heat transport across the North Sea boundary the term $u_\perp(T - T_{\mathrm{ref}})$ in $\mathrm{OHT}_{\mathrm{adv}}$ is replaced by the following decomposition:

$$\begin{aligned}u_\perp(T - T_{\mathrm{ref}}) =& \overline{u}_\perp(T - T_{\mathrm{ref}})' + u'_\perp\overline{(T - T_{\mathrm{ref}})} \\ &+ u'_\perp(T - T_{\mathrm{ref}})' \qquad (4)\end{aligned}$$

The bar denotes the time mean (1993–2022) and the prime an anomaly from the mean. $\overline{u}_\perp(T - T_{\mathrm{ref}})'$ represents changes of the inflow temperature relative to the domain interior in the presence of a mean flow. $u'_\perp\overline{(T - T_{\mathrm{ref}})}$ represents circulation changes in the presence of a mean temperature difference between the exterior and interior of the domain. The last term on the right hand side is related to the covariance of temperature and circulation anomalies.

3.2.3 Definition of pressure & climate indices

To relate temperature variability and the occurrence of MHWs to larger-scale patterns of oceanic and atmospheric variability we use different climate indices that have been linked to MHWs in the North Sea (Mohamed et al., 2023; Lin et al., 2025; Mohamed et al., 2025). The North Atlantic Oscillation (NAO) and East Atlantic Pattern (EAP) indices are obtained from the NOAA Climate Prediction Center (https://www.cpc.ncep.noaa.gov/products/precip/CWlink/pna/nao.shtml, last access: 9 July 2025; https://www.cpc.ncep.noaa.gov/data/teledoc/ea.shtml, last access: 9 July 2025). Both indices represent similar patterns in the sea-level pressure, but with different centers of action. The EAP is especially important in setting the wind direction over the North Sea (Chafik et al., 2017; Lin et al., 2025). The El Niño Southern Oscillation (ENSO) Index used here is derived from HadISST (Rayner et al., 2003) temperature in the Niño3.4 region and provided by the NOAA Physical Sciences Laboratory (https://psl.noaa.gov/data/timeseries/month/, last access: 29 July 2025). We also use the Atlantic Multidecadal Variability (AMV) index obtained from the Climate Analysis Section of NCAR (https://climatedataguide.ucar.edu/climate-data/atlantic-multi-decadal-oscillation-amo, last access: 9 July 2025).

The AMV index is detrended over the same period as the temperature (detrended baseline period: 1993–2023) before further analysis. The AMV reflects the temperature of the North Atlantic and we aim to investigate whether a warm North Atlantic coincides with a warm North Sea and more MHWs relative to a detrended baseline. For the NAO, EAP and ENSO only the mean was removed, because we assume these climate indices are related to the heat fluxes (i.e. temperature change) not absolute temperature.

In addition to the well established climate indices, we define new pressure-based indices (P_i) for each season. These indices are defined to maximize their correlation with the season mean net heat flux (heat content change) in the German Bight. The indices are always based on the pressure difference between two locations, a and b, and calculated as follows:

$$P_i = (P_a - \overline{P}_a)/\sigma_{P_a} - (P_b - \overline{P}_b)/\sigma_{P_b} \tag{5}$$

where P_a and P_b are the sea level pressure at the two given locations. The bar denotes the time mean and σ the standard deviation.

3.3 Conditional probabilities

Relationships between the occurrence of MHWs and the climate indices (and other variables) on seasonal timescales were identified based on conditional probabilities. Note that simply calculating correlations between the indices and the number of MHW days, for example, is not possible, because the number of MHW days is bounded by zero. Even if there would be a strong relationship it cannot be expected to be linear. A strongly negative state of a climate index would not lead to fewer MHW days compared to a neutral state, when the neutral state is already associated with zero MHW days. Instead we calculate the probability of at least one MHW to occur in a season, given that the season mean climate index exceeds its standard deviation (p_{11}). Likewise, we calculate the probability that a MHW occurs, given the climate index does not exceed one standard deviation (p_{10}). The contingency tables are completed with the inverse probabilities (p_{01} and p_{00}). We then apply Fisher's exact test to the contingency table to test the null hypothesis that the two input variables (occurrence of MHWs and positive state of climate indices) are independent. The null hypothesis is rejected (i.e. the input variables are considered to be related) when the p-value is smaller than 0.05 (5 % significance level).

3.4 Linear regression model

To identify linear relationships between the season mean temperature anomalies and the climate and pressure indices we apply a linear model defined by:

$$\hat{y}(t) = a_1 x_1(t) + a_2 x_2(t) + \ldots + a_n x_n(t) \tag{6}$$

$\hat{y}$ is the predicted variable. The coefficients of the linear model (a) are estimated by minimizing the residual sum of squares between the predicted $\hat{y}$ and observed values y using the scikit-learn python package (Pedregosa et al., 2011). y is the season mean temperature anomaly in our study. x are the predictor variables, for example a climate or pressure index.

3.5 Significance of trends and correlations

The linear trend is calculated as the slope of the linear regression (Eq. 6 with one input variable). The p-value is estimated from a two-sided t-test.

$$p = 2(1 - F_t(|t_\mathrm{s}|;\ \mathrm{d}f = n-2)) \tag{7}$$

F_t is the cumulative distribution function of the t-distribution with $n-2$ degrees of freedom. n is the length of the timeseries. t_s is the test statistic given by:

$$t_\mathrm{s} = \frac{a_1}{\mathrm{SE}_{a_1}} \tag{8}$$

with SE_{a_1} being the standard error of the slope a_1.

For the Pearson correlation coefficient (r) we calculate the p-value as in Eq. (7), but the test statistic is given by:

$$t_\mathrm{s} = r\sqrt{\frac{n-2}{1-r^2}} \tag{9}$$

To account for autocorrelation in the timeseries (i.e. non-independent time steps) when calculating the correlations we replace n by the effective sample size (n_eff) calculated following Thomson and Emery (2014).

In both cases, the null hypothesis of the linear trend or correlation coefficient being zero is rejected if the p-value is smaller than 0.05 (5 % significance level).

4 Past evolution of MHWs in the North Sea

When averaged over the entire North Sea all datasets show a similar past evolution of MHW characteristics (Fig. 1). Although the timeseries show the full extent of the datasets, the mean and trend are calculated for the years 1993 to 2023 to allow for a comparison. All datasets show a very similar mean, temporal evolution, and trend for commonly analysed characteristics of MHWs (here: MHW days and maximum intensity).

On average, about 1.7 MHWs, lasting 15 d, occur per year at each location in the North Sea, which results in about 26 MHW days per year independent of the baseline used (Fig. 1a, b). V20 and the reanalysis products overestimate the duration by about 3 d compared to the satellite products. This results in 3–4 more MHW days per year for both baselines. In part, this difference could be explained by the satellite datasets representing a foundation temperature (without a diurnal cycle; Good et al., 2020), while the model-based datasets usually simulate the diurnal cycle. This will cause the temperature to rise stronger in the model datasets because one would expect an amplification of the diurnal cycle during surface-forced MHWs (at least for shortwave driven heatwaves). Nevertheless, the diurnal cycle is strongly smoothed, because of the limited vertical model resolution. Furthermore, the difference in MHW days between the datasets is much smaller than the interannual standard deviation (errorbars in Fig. 1a, b).

As evident from the timeseries (Fig. 1a, b) and their correlation (Fig. 1c), the timing of variability is very similar in all datasets. OIS shows the overall lowest correlation to other datasets, but the correlation exceeds 0.93 between any pair of datasets. All correlations are significantly different from 0 at a significance level of 5 %. Correlations are only shown here for the detrended baseline, but are very similar for the fixed baseline.

Differences in mean and variability are more pronounced for the maximum intensity, where V20 and G12 simulate weaker (1.7–1.9 °C) MHWs compared to the other datasets (> 2.2 °C; Fig. 1d, e). Similar differences are seen for both baselines. The correlation is still very high between the satellite products (> 0.8), but slightly lower for correlations involving the model and reanalysis datasets (Fig. 1f). Nevertheless, all correlations exceed 0.67 and are significantly different from 0 at a significance level of 5 %.

All datasets agree on significant positive trends in the North Sea temperature between 0.24 °C per 10 years in V20 and 0.37 °C per 10 years in OIS. Consistently, the number of MHW days, frequency, and duration show a positive trend in all datasets when a fixed baseline is used (Table 2). OIS shows the highest and most significant trends (lowest p-values) for all quantities, except maximum intensity. Trends in datasets other than OIS are only statistically significant for the frequency of MHWs. The maximum intensity shows non-significant negative trends in all datasets, except NWS where the linear regression slope is 0. With the detrended baseline, trends in all variables and datasets considered here are non-significant (not shown).

4.1 Regional differences in the past evolution of MHWs

Although trends in the number of MHW days and intensity are not significant in most datasets when averaged over all grid points in the North Sea, there are regions with significant trends (Fig. 2a–d). The number of MHWs increases in all datasets (V20, NWS, OIS and OST are shown here as examples) in the Southern Bight (near the entrance to the English Channel) and along the UK east coast. In the model based datasets a significant increase extends into the Dogger Bank region, while in OST significant increases are confined more to the English Channel. OIS shows stronger trends throughout the entire North Sea, but the pattern is similar to the other datasets, with a stronger increase in the Southern Bight and along the UK east coast. Although mostly not significant, an increase is also visible in the German Bight. While in the Southern Bight both, duration and frequency have increased, in the German Bight only the frequency has increased (not shown). Parts of the northern North Sea experienced an increase in frequency, but a decrease in duration, resulting in no change in MHW days.

The maximum intensity shows even more pronounced regional differences. A small part along the French and Dutch coast experienced a significant increase, but most of German Bight and central North Sea show a decrease in the maximum intensity (Fig. 2e–h). This is interesting as the temperature shows a significant positive trend throughout the entire North Sea, which is largest in the German Bight (Fig. 2i–l). Although not significant, even in OIS the maximum intensity decreases, despite strong increasing trends in all other variables (including temperature).

4.2 Changes in the German Bight's temperature distribution

The strong change in mean temperature in the German Bight would have led to many more MHW days and more extreme temperature anomalies (i.e. an increase in maximum intensity), had the distribution simply shifted to higher values. However, this is not visible in the characteristics of MHWs (see previous sections). In particular in the German Bight, where the temperature trend is strongest, the number of MHW days did not become significantly larger and the intensity even decreased. Indeed all datasets suggest that the distribution of temperature anomalies has not just shifted, but also changed in width (standard deviation). We have only selected two datasets for an in-depth analysis here to keep the results concise (Fig. 3). We use the OST satellite product, because it is commonly used to study MHWs in the North Sea and V20, because it provides the most comprehensive dataset

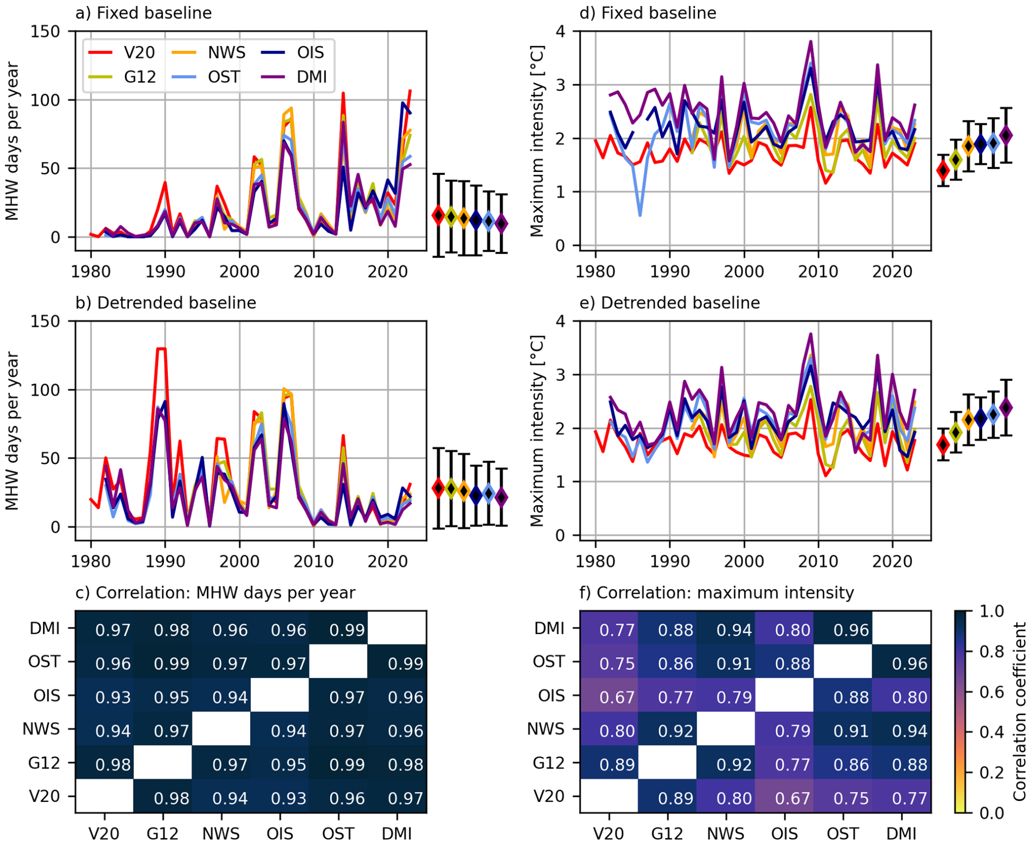

c) Correlation: MHW days per year

	V20	G12	NWS	OIS	OST	DMI
DMI	0.97	0.98	0.96	0.96	0.99	
OST	0.96	0.99	0.97	0.97		0.99
OIS	0.93	0.95	0.94		0.97	0.96
NWS	0.94	0.97		0.94	0.97	0.96
G12	0.98		0.97	0.95	0.99	0.98
V20		0.98	0.94	0.93	0.96	0.97

f) Correlation: maximum intensity

	V20	G12	NWS	OIS	OST	DMI
DMI	0.77	0.88	0.94	0.80	0.96	
OST	0.75	0.86	0.91	0.88		0.96
OIS	0.67	0.77	0.79		0.88	0.80
NWS	0.80	0.92		0.79	0.91	0.94
G12	0.89		0.92	0.77	0.86	0.88
V20		0.89	0.80	0.67	0.75	0.77

Figure 1. Number of marine heatwave days per year (left) and annual mean maximum intensity (right) averaged over the North Sea (fixed baseline: **a, d**; detrended baseline: **b, e**). Diamonds and errorbars indicate the 1993–2023 mean and standard deviation. Correlation between the annual timeseries of MHW days **(c)** and maximum intensity **(f)** from different datasets (detrended baseline).

Table 2. Linear trend (1993–2023) in North Sea temperature, MHW frequency, duration and maximum intensity (fixed baseline; averaged over the entire North Sea) derived from different datasets. Bold values indicate slopes significant at the 5 % level.

	Temperature [°C per 10 years]	MHW days [Days per 10 years]	Frequency [MHWs per 10 years]	Duration [Days per 10 years]	Max. intensity [°C per 10 years]
V20	**0.24**	11.2	**0.50**	1.63	−0.04
G12	**0.26**	8.9	0.48	1.45	−0.02
NWS	**0.27**	9.0	0.51	1.30	0.00
OIS	**0.37**	**14.8**	**0.87**	**1.90**	−0.04
OST	**0.31**	8.5	**0.62**	0.73	−0.02
DMI	**0.34**	8	**0.56**	0.88	−0.05

available to us (including for example 3D ocean currents and temperatures as well as all heat flux components).

In order to study temporal changes in the distribution we calculate the mean and standard deviation of the distribution of temperature anomalies in the German Bight within 5-year windows (Fig. 3). Anomalies are defined relative to the fixed and detrended baselines as for the MHW detection. We focus on MHWs detected in the German Bight here, as changes in the shape of the temperature distribution were most pronounced for this region. The MHW statistics for the German Bight are derived from the region's mean temperature, as described in the methods section.

Relative to the fixed baseline, the German Bight became about 2 °C warmer than in the early 1980s in all seasons (Fig. 3a–e). As expected, a higher mean leads to more extremes (MHWs) by shifting the temperature distribution towards higher values.

The North Sea did not just experience a long-term warming trend, but the temperature also varies relative to the trend. This is seen with the fixed baseline, but is better visible when

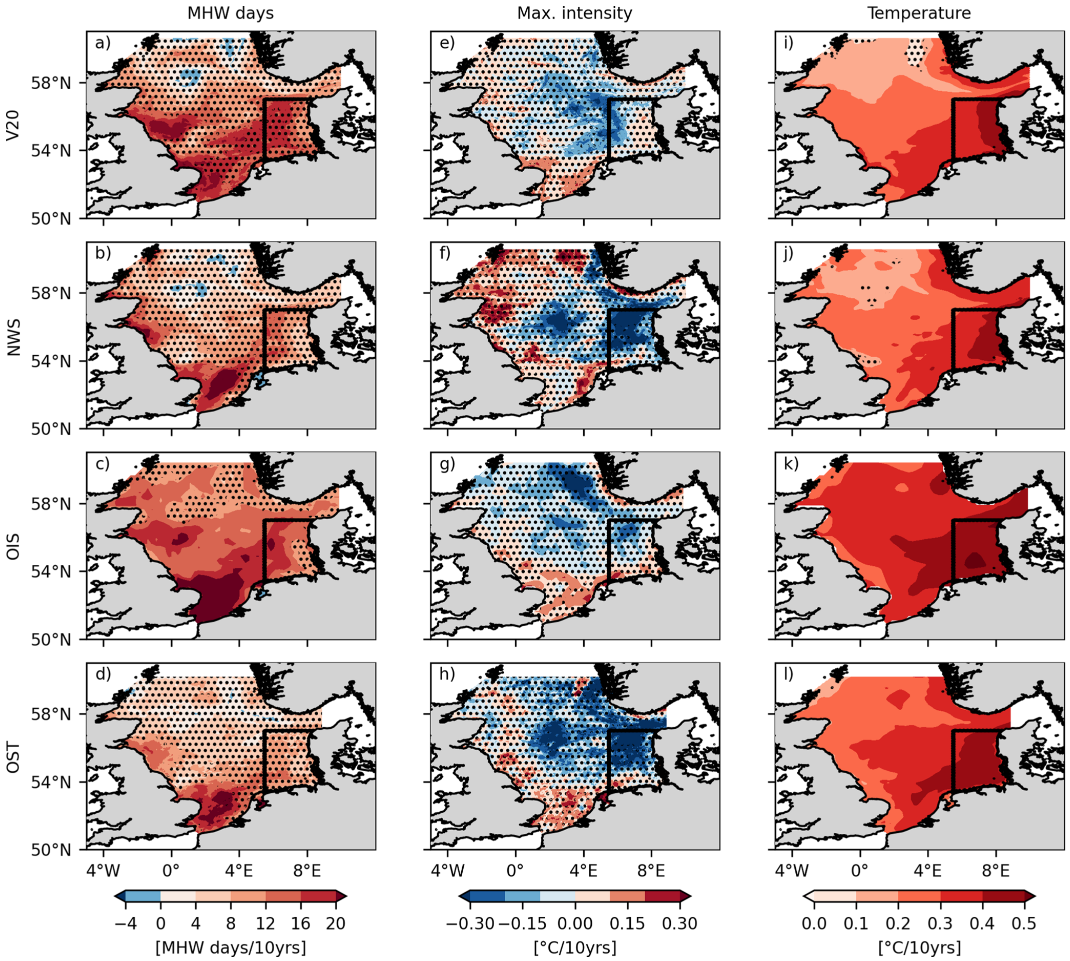

Figure 2. Linear trends (1993–2023) in MHW days per year **(a–d)**, maximum intensity **(e–h)** and temperature **(i–l)** in VIKING20X, the European Northwest Shelf reanalysis, OISST and OSTIA. Non-significant slopes based on a significance level of 5 % are indicated by dots.

considering temperature anomalies relative to the linear trend (detrended baseline; Fig. 3f–j). While the years 1989–1993 and 1999–2008 were anomalously warm, the years 1984–1988 and 2009–2013 were anomalously cold.

In contrast to the mean, the standard deviation does not show a significant trend with either baseline, but is dominated by variability on shorter timescales. A strong peak in standard deviation occurred in 1994–1998. Especially in winter and spring the mean temperature was below average relative to both baselines, but still a considerable amount of MHW days occurred (Fig. 3b, c, g, h). In other years, a lower standard deviation led to fewer extremes than expected from the mean temperature anomaly. For example the period 1999–2003 shows a similar mean temperature anomaly as 2004–2008, but fewer MHW days (Fig. 3a). This change was particularly pronounced in spring (Fig. 3c). In winter, changes in the mean were much more important than changes in standard deviation (Fig. 3b). Anomalies in the mean and standard deviation are not strongly dependent on the season, but their relative importance may differ across seasons.

The characteristics of MHWs show a pronounced seasonal cycle in most datasets used in this study. Most MHW days occur in summer and fall, and fewer MHW days in winter and spring (Fig. A1a). The seasonal cycle in MHW days exhibits a larger amplitude in the satellite datasets compared to the reanalysis datasets and especially compared to the VIKING20X model. This is caused by too long MHWs in winter and too few MHWs in summer (not shown). The maximum intensity of MHWs peaks in spring and summer, with MHWs being up to 1.2 °C more intense compared to fall and winter (Fig. A1b). VIKING20X fails to simulate this increase in spring/summer intensity, but shows almost the same intensity in all seasons. The reason for this is related to the vertical structure of MHWs and investigated in detail later. An interesting feature of the seasonal timeseries (here V20 and OST are shown as examples) is that the recent years (2019–2023) show the highest temperature anomaly relative to the fixed baseline, but not the most MHW days (Fig. 3a). This is caused by a negative anomaly in standard deviation. Additionally, the temperature was below average relative to

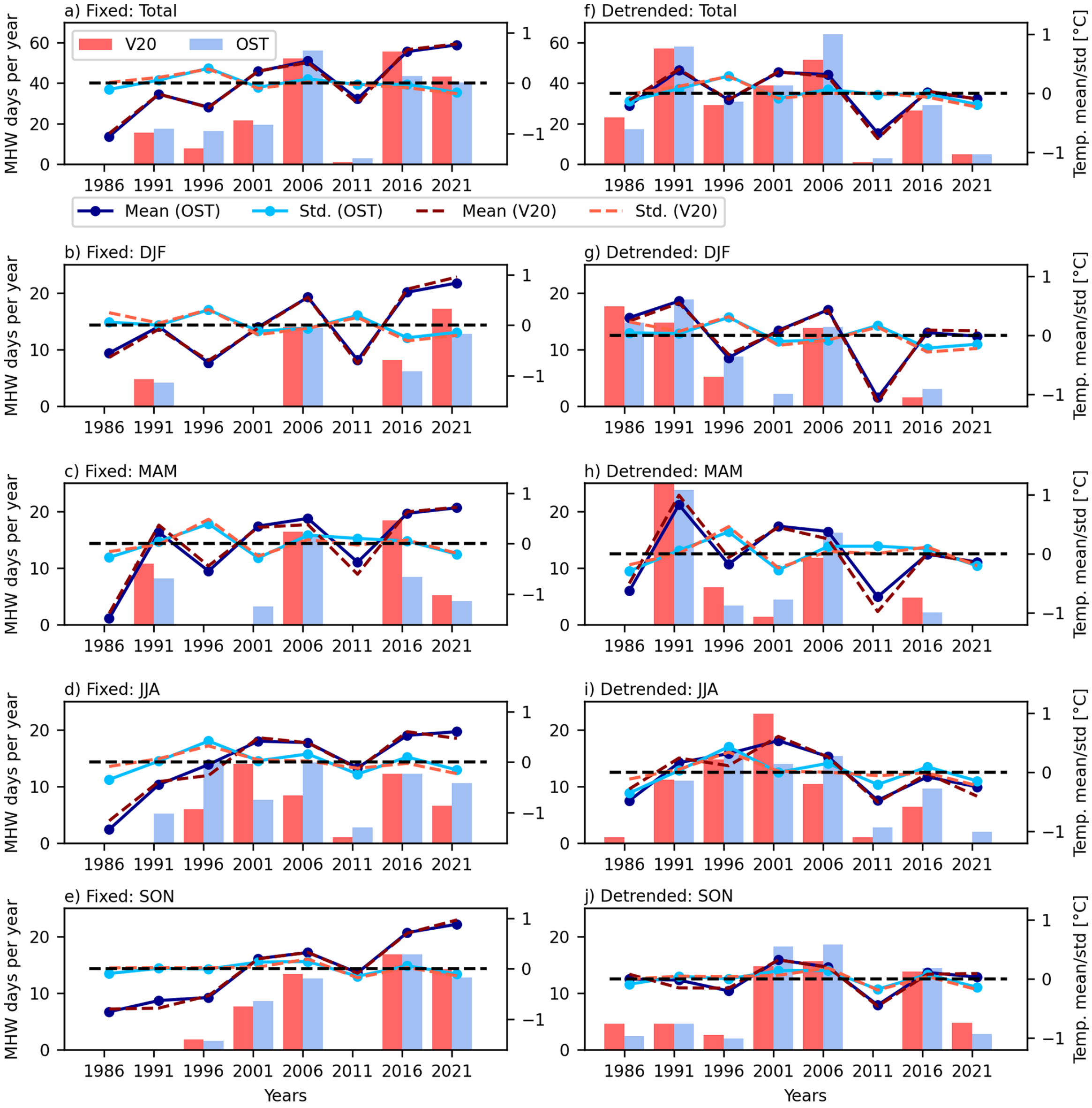

Figure 3. Average number of marine heatwave days per year (bars) in 5-year windows from VIKING20X and OSTIA (fixed baseline: **a–e**; detrended baseline: **f–j**) in the German Bight. Labels on the x-axis indicate the center of the window. The mean temperature and standard deviation anomalies in the same 5-year windows are shown as lines. Panels **(a)** and **(f)** consider all days within the window, while panels **(b)**–**(f)** and **(g)**–**(j)** only those from the indicated months.

the linear trend (Fig. 3f), leading to almost no MHWs relative to the detrended baseline. While the standard deviation was smaller in all seasons, the mean was below average only in spring and summer (Fig. 3g–j). Both resulted in fewer extremes than expected from the linear long-term warming trend in the German Bight. The reduced standard deviation can also explain why the maximum intensity of MHWs showed a decreasing tendency, even with the fixed baseline. Despite a higher mean temperature, a lower standard deviation reduces the magnitude of the highest temperature anomalies reached.

All results are equally valid for both the V20 and OST datasets. The temporal evolution of the mean is similar between the two datasets, and the same holds for the standard deviation. The number of MHW days can slightly differ within the seasons, but usually show the same change between consecutive 5-year periods (Fig. 3b–e, g–j). The number of MHW days is very similar when the entire year is considered (Fig. 3a, f).

5 Atmospheric and oceanic conditions during MHWs in the German Bight

The conditions during MHW events are studied in more detail using the VIKING20X model output, since it provides a comprehensive and physically consistent ocean and atmospheric state during MHWs. To ensure that we do not analyse events that were only simulated in the model but did not occur in the real ocean, we only consider validated MHW events (see methods). VIKING20X simulates 34/49 validated events with the fixed/detrended baseline and 7/19 events that are not validated. The model misses about 16/11 events that are simulated by multiple satellite-based datasets. However, as two separate MHWs in the satellite observations are often merged to a single event in VIKING20X, which is consistent with the bias in duration, most of the MHW periods are simulated as such in VIKING20X (81 %/84 % of the validated MHW days are correctly simulated as MHW days in VIKING20X).

5.1 Main drivers of MHWs

MHWs in the German Bight can be driven by either a convergence of the oceanic heat transport, or by a heat gain through air-sea heat fluxes. The latter can be caused by any of the individual heat flux components (latent: LA, sensible: SE, shortwave: SW or longwave: LW), or a combination. In most months the surface heat flux contribution dominates the development of MHWs (Fig. 4a, d). Nevertheless, the oceanic heat transport does contribute to events as well. For fixed baseline events, the OHT contributes in October, February, and March (up to 75 %). With the detrended baseline, it contributes most strongly in November, December and February (up to 55 %). From May to August the OHT contribution is close to zero or slightly negative for both baselines, meaning it damps the development of MHWs.

For both baselines the SW flux is the dominant driver of MHWs from May to June (Fig. 4b, e). Additionally, with the detrended baseline the SW flux is the dominant driver of MHWs in August. Most MHWs are either driven by SW alone, or a combination of SW and LA. From August to October, the main driver of most events is an anomalous latent heat flux into the ocean (less evaporative cooling). In winter and spring the results are more baseline-dependent. The ocean heat transport is important with the detrended baseline in November and December, while with the fixed baseline all events in these months are predominantly driven by a combination of the sensible and latent heat fluxes. In February and March MHWs are exclusively driven by the OHT with the fixed baseline, while latent heat flux and sensible heat fluxes play a more important role with the detrended baseline.

For the fixed baseline, MHWs driven by a specific process are scattered across the timeseries. The same is true for SW-driven MHWs with the detrended baseline (Fig. 4c, f). In contrast, OHT and latent heat driven MHWs tend to cluster for the detrended baseline (Fig. 4f). Most OHT driven MHWs occurred between 1987 and 1995 and most latent heat driven MHWs between 1998 and 2006 (and additionally multiple events in 2014).

5.2 Composite conditions during the onset of MHWs

The different drivers of MHWs (here fixed baseline) are associated with distinct atmospheric circulation patterns. We focus on the most frequent types of events here (OHT, SW + LA and LA). Due to their similarity (not shown), SW and SW + LA driven MHWs were grouped together. In addition to the surface conditions, we also investigate the vertical profiles of temperature anomalies during the MHW events.

OHT-driven MHWs (five events) that occur in fall and winter are linked to a low pressure system located northwest of the British Isle (Fig. 5a). The north-south pressure gradient is increased over the English Channel, driving strong wind stress anomalies that increase the inflow of warm water from the Atlantic Ocean into the southern North Sea. The warm water spreads along the southern North Sea coast and causes strong temperature anomalies in the German Bight (Fig. 5a, b). Transport-driven MHWs show an almost flat vertical profile with little variations in the temperature anomaly from the surface to 40 m depth (Fig. A2a–c). Thus for the majority of the German Bight region, the temperature anomaly is similar at the surface and at the bottom. This is expected since these MHWs are driven by barotropic transport anomalies and accompanied by strong winds that cause vertical mixing (Fig. 5a, b). V20 shows temperature anomalies very similar to those in the other datasets. Note that three different baseline periods are used here because the CST1 and BSH datasets do not cover the same period as the other datasets. The BSH, CST1, G12 and V20 datasets all show very similar profiles, while NWS and the satellite data suggest weaker anomalies for events after 2016 (Fig. A2b, c). However, only one OHT-driven MHW occurred after 2016 (Fig. 4c).

Shortwave (+ latent) heat flux driven MHWs (twelve events) that usually occur in the summer months are associated with a high pressure system located over Scandinavia, which leads to low cloud cover (thus high solar insolation) and weak winds over the German Bight. In contrast to the OHT driven MHWs, strong temperature anomalies are not limited to the southern part, but extend across the entire North Sea (Fig. 5c, d). Shortwave driven MHWs are characterized by a shallow mixed layer of only a few meters depth (Fig. A2d–f). The high-resolution BSH model and the two reanalysis products simulate a steep temperature gradient in the top 10 m. Consistent with the atmospheric conditions (Fig. 5c, d), the incoming shortwave heat flux is distributed over a small volume and therefore leads to high temperature anomalies in the top meters of the water column. Even in the presence of tidal forcing (BSH and NWS) the shallow parts of the German Bight are not fully mixed in the model and a thermocline can develop (Fig. A2d–f). The surface anomalies

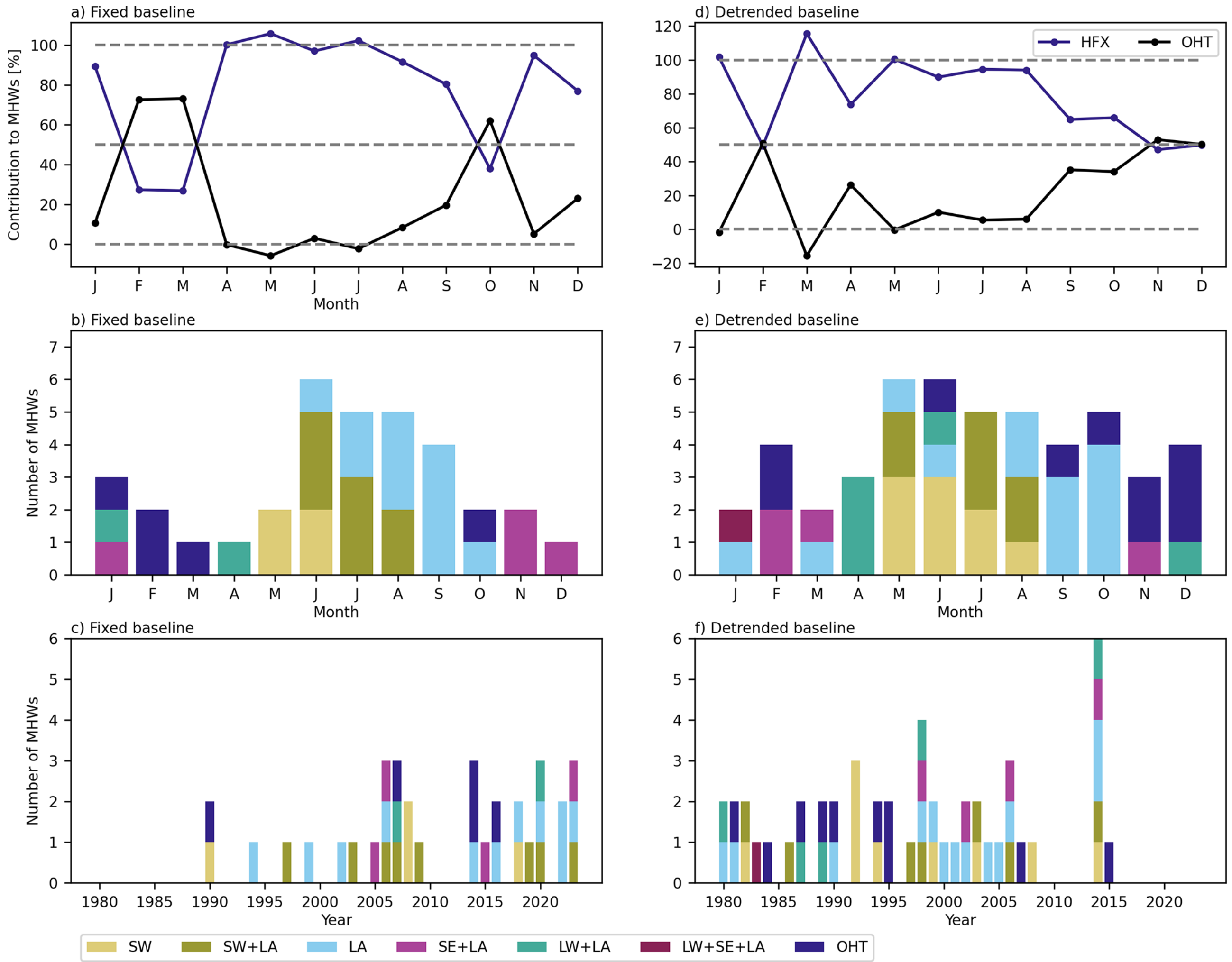

Figure 4. Contribution of the local surface heat flux (HFX) and oceanic heat transport (OHT) convergence to the development of MHWs in the German Bight detected with the fixed **(a)** and detrended **(d)** baselines in each month. Total number of MHWs driven by a specific process in each month **(b, e)**. The sum of all bars adds up to the total number of validated MHWs between 1982 and 2023. Timeseries indicating the dominant drivers of all MHWs detected in a respective year **(c, f)**. The heat flux was decomposed into the contribution of the shortwave (SW), longwave (LW) sensible (SE) and latent (LA) heat flux.

are very similar in NWS, BSH, and the satellite observations. G12 slightly underestimates the temperature anomaly. V20 cannot simulate such shallow mixed layers, due to its limited vertical resolution. The uppermost level represents a mean temperature of the upper 6 m and cannot capture variations within this depth range. As a consequence, the heat gained at the surface is distributed over a too large volume, causing the MHW intensity in summer to be underestimated at the surface (see Fig. A1b). At deeper levels the temperature anomalies in V20 generally match those from the other datasets. An important role of the vertical resolution is supported by a very similar temperature profile in CST1 (Fig. A2f). CST1 is based on a very different model set-up (e.g. including tides, different surface forcing), but shares a similar vertical resolution compared to V20. Below 20 m depth the temperature anomaly is close to zero relative to the 1993–2023 baseline, suggesting a decoupling of surface and bottom MHWs in deeper parts of the German Bight (mostly in the northern part of the area).

Latent heat driven MHWs (eleven events) that often occur in fall are associated with low pressure west of the British Isles and high pressure over Scandinavia or the Baltic Sea. Similar to SW-driven MHWs, positive temperature anomalies can be seen throughout most of the North Sea (Fig. 5e, f). Winds are weak and blow from south to southeast. As the air masses circulate counter-clockwise around the low pressure system, they bring moist air from the Atlantic to the North Sea. Together with the low wind speed, this leads to highly saturated air close to the sea surface, which reduces evaporation and thus the latent heat loss from the ocean to the at-

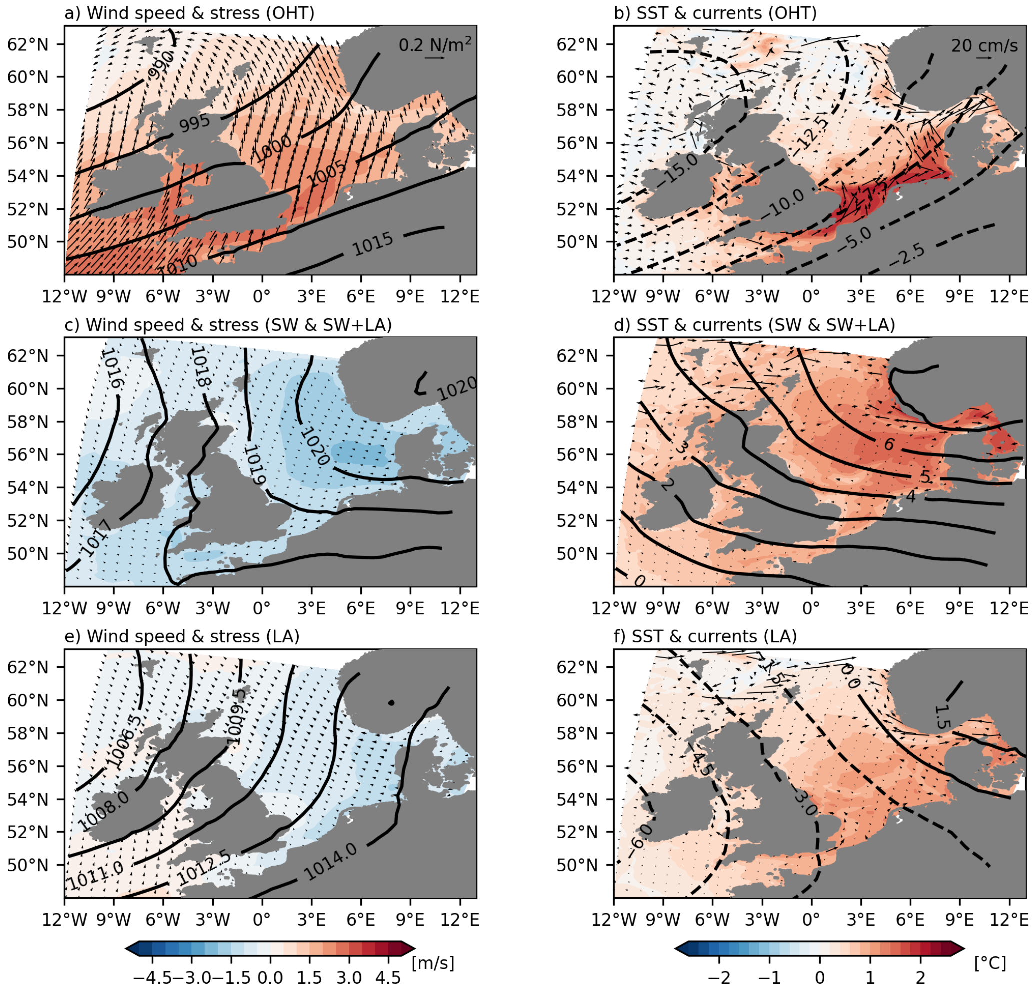

Figure 5. Mean oceanic and atmospheric conditions during the onset of MHWs in the German Bight (fixed baseline) driven by the ocean heat transport **(a, b)**, shortwave or shortwave and latent heat flux **(c, d)** and latent heat flux alone **(e, f)**. All maps show the composite of all MHWs that were attributed to the mentioned drivers (see methods for details). Contours show the air pressure in hPa **(a, c, e)** or the air pressure anomaly **(b, d, f)**. Arrows show the wind stress anomaly **(a, c, e)** and surface current anomaly **(b, d, f)**. Shading shows the wind speed anomaly **(a, c, e)** and sea surface temperature anomaly **(b, d, f)**.

mosphere. Similar to SW-driven MHWs, LA-driven MHWs show the highest temperature anomalies of 1.5 °C at the surface. Compared to the SW driven MHWs the anomaly decreases more gradually to 0.5 °C in 30 m depth (Fig. A2g–i). This is again consistent with relatively weak winds and a strong heat flux anomaly at the ocean's surface (in this case due to reduced evaporative cooling). Note that depths beyond 30 m are only reached in the northern part of the German Bight region as it is defined here. Again, the BSH model shows a slightly stronger, V20 and CST1 a weaker, vertical temperature gradient compared to the reanalysis products.

These results show that the occurrence of MHWs is linked to specific weather patterns. The main drivers of MHWs depend on the season (Fig. 4b, e) and so do the corresponding weather patterns (Fig. 5). Both the timeseries (Fig. 4c) and the composites (Fig. 5) suggest that the long-term warming trend in the North Sea did not lead to a considerable change in the main drivers of MHWs over time. In general, the identified atmospheric patterns do not depend on the baseline. The same weather patterns drive MHWs detected with the detrended baseline (Fig. A3), even though these MHWs appear at different times (Fig. 4c, f). This suggests that the occurrence of a specific weather pattern alone is not sufficient to trigger a MHW, but variability on longer timescales is important as well. This will be investigated in more detail in a later section.

5.3 Advective MHWs: extreme or rare conditions

As the conditions for summer MHWs have already been studied (Mohamed et al., 2025; Berthou et al., 2024), we focus on the advective-driven MHWs (fall and winter) here. These heatwaves are associated with a low pressure system north of the British Isles (Fig. 5a, b), but neither the low pressure system nor the heat transport anomalies into the German Bight need to be exceptionally strong to trigger a MHW. This is illustrated by three examples (Fig. 6).

In 1990 a low pressure system over Scotland caused strong wind anomalies over the English Channel (Fig. 6a), which resulted in a strong heat transport anomaly (Fig. A4: black lines). However, the negative surface heat flux anomaly (ocean heat loss) damps the transport anomaly throughout the entire southern North Sea, preventing a MHW (Fig. 6b).

Another mechanism is seen in 2009. The wind speed (Fig. 6e) and inflow (Fig. A4: blue lines) anomalies in the English Channel are even stronger and more persistent than in 1990. The heat flux anomaly in the German Bight is positive and therefore also contributes to a warming (Fig. 6d). Still, no MHW is detected in the German Bight. This is caused by an initially cold ocean (relative to both baselines; Figs. 6f and A4b, c). In late summer 2009 the German Bight was about 1.5 °C colder than the climatology. On 14 November, when the shown low pressure system reached the North Sea the temperature anomaly was close to zero relative to the detrended baseline (Fig. 6f). Thus, the very strong anomalies in 2009 caused a strong increase in the temperature of the German Bight, but did not lead to a MHW (Fig. A4b, d).

In 1995 a low pressure system northwest of Scotland (upper left boundary of the map) led to an increased pressure gradient and slightly stronger than average southwesterly winds over the English Channel (Fig. 6g, h). Neither the low pressure system itself, nor the wind anomalies, nor the heat transport anomalies in the southern North Sea were particularly strong or sustained for an unusually long time (Fig. A4: red lines). Still, a MHW developed from the relatively small heat inflow anomaly (with a minor contribution from the surface heat flux), as the temperature was already close to the MHW threshold before (Figs. 6i and A4c). This initial anomaly was caused by a stronger low pressure system that passed the northern North Sea about 20 d prior to the MHW onset (Fig. A4a: red line around day 280).

This shows that advective MHWs in the German Bight are driven by a rare combination of preconditioning, inflow, and heat flux anomalies rather than extreme atmospheric conditions (e.g. a very strong low pressure system close to the British Isles). The preconditioning factor is strongly influenced by the chosen baseline, while the change in temperature is independent of the baseline (Fig. A4b, c). With the detrended baseline the temperature was close to the MHW threshold when the second low pressure system passed on day 300, while it was just above the climatology for the fixed baseline. The same warming then raised the temperature above the MHW threshold for the detrended baseline, but barely above the climatology with the fixed baseline.

6 Ocean preconditioning in the German Bight

Since the initial temperature of the ocean when a specific weather pattern occurs plays a major role for the development of MHWs, we investigate causes of temperature changes in the German Bight on different timescales and how MHWs are related to different climate indices. If the entire water column is considered, the temperature in the German Bight, or equivalently the heat content, can be changed by either a convergence of the oceanic heat transport or by the surface heat flux.

6.1 Variability on seasonal timescales

As the number of MHW days is bounded by zero, a linear relation (i.e. correlation) to the other timeseries cannot be expected. Instead, we calculate the conditional probabilities of at least one MHW occuring in a season, dependent on a given state of other variables. We group the months by the dominant processes that cause MHWs (Fig. 4), as we expect similar atmospheric patterns to be associated with a warming/-cooling of the German Bight. These are winter (JFM), summer (MJJ), early fall (ASO) and late fall (ND). The month of April is not contained by any group, because it is a transition month and does not fit the winter nor the summer group.

In all seasons the occurrence of MHWs is strongly related to the season mean temperature anomaly, even though MHWs themselves can be as short as 5 d and do not necessarily cause an above average season mean temperature (Fig. 7a).

Although the surface heat flux is significantly correlated to the NAO in most months, except early fall (Fig. A5), an anomalously positive NAO index is not related to a higher probability of MHWs occurrence (Fig. 7b). In summer there is a significant negative correlation to the heat transport convergence, because a local heating of the German Bight by surface heat fluxes increases the temperature of the outflow across the northern boundary (Fig. A5).

The EAP is significantly correlated to the heat transport convergence in all seasons except summer (Fig. A5). Thus, in contrast to the NAO, the EAP influences the heat budget by changing the (wind-driven) oceanic circulation rather than the atmospheric conditions alone. For both heat transport convergence and heat content change correlations to the EAP are similar year round, with values of 0.4–0.5 for the convergence and 0.2–0.4 for the net heat flux (p-values are close to 0.05). In late fall and winter the EAP strongly controls the heat transport along the southern boundary of the North Sea from the English Channel to the western boundary of the German Bight. In late summer the EAP index is not significantly correlated to the heat transport across the western, but the northern, boundary of the German Bight (Fig. A5). Still, only in winter MHWs are significantly more likely to occur given that the EAP is in a positive state (Fig. 7c). The same is

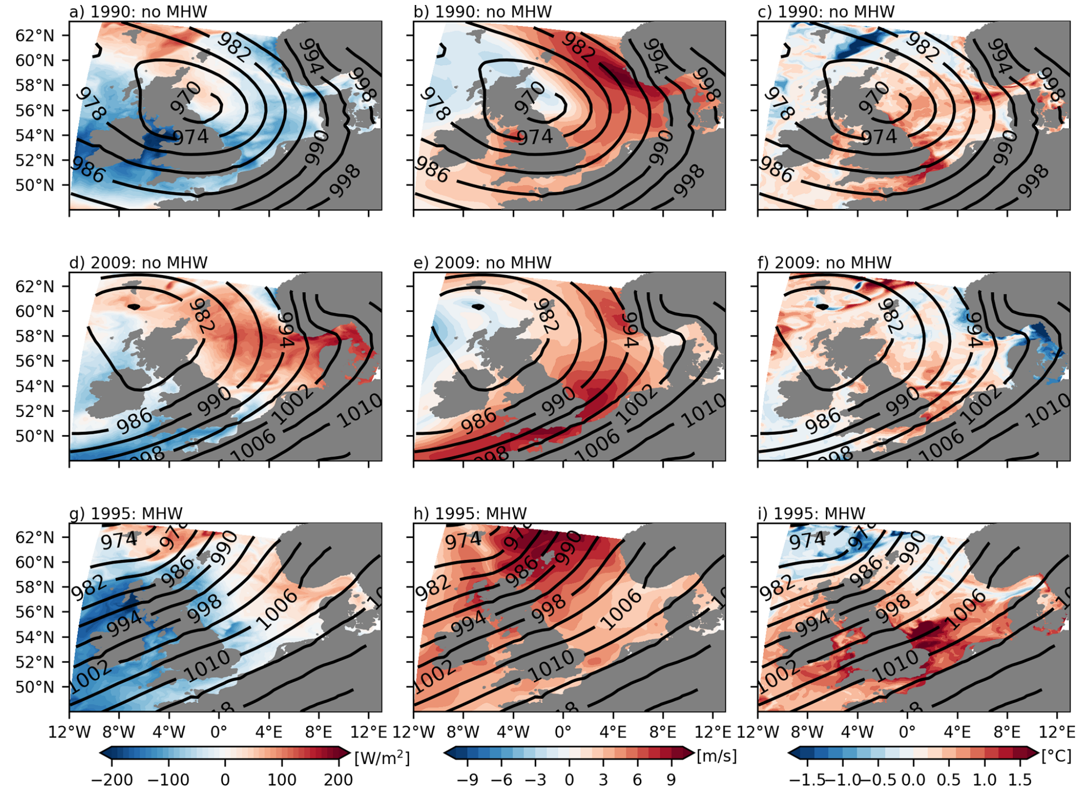

Figure 6. Daily mean surface heat flux **(a, d, g)**, wind speed anomaly **(b, e, h)** and temperature anomaly relative to the detrended baseline **(c, f, i)** along with air pressure contours. All days (28 October 1990: **a–c**; 14 November 2009: **d–f**; 26 October 1995: **g–i**) are associated with local maxima in the heat transport through the English Channel, but only in 1995 a MHW was triggered in the German Bight.

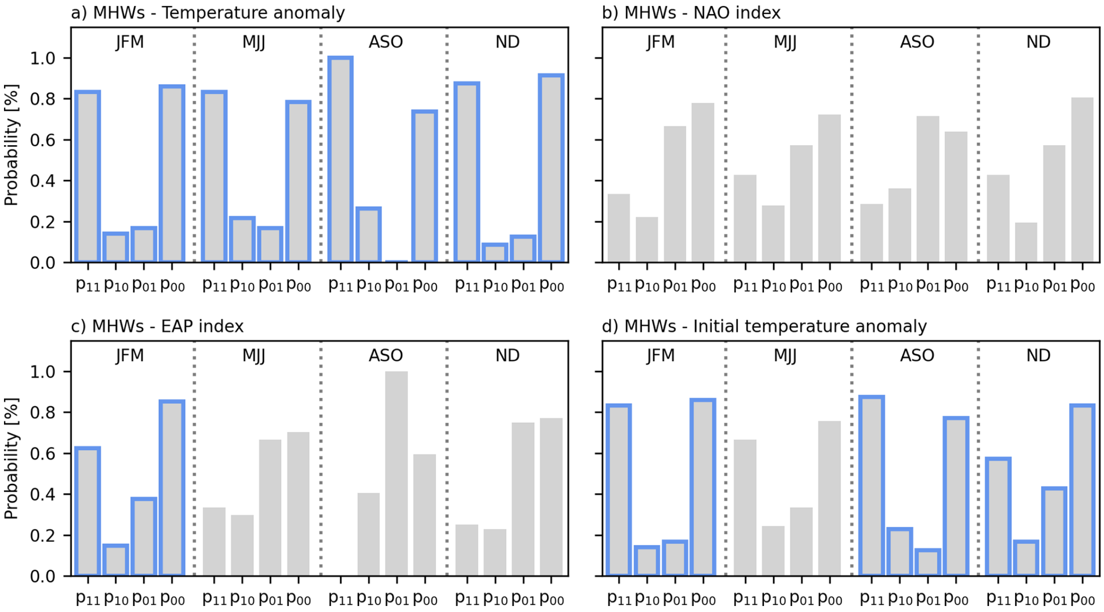

Figure 7. Conditional probabilities dependent on the season in the German Bight region. p_{11}/p_{10} – Probability of at least one MHW given the selected index exceeds/does not exceed one standard deviation. p_{01}/p_{00} – Probability of no MHW given the selected index exceeds/does not exceed one standard deviation. If the null hypothesis of the two input variables being independent is rejected based on a 5 % significance level, the bars are marked with a blue outline.

true for the probabilities of MHWs given the NAO and EAP are anomalously positive at the same time (not shown).

The ENSO index is significantly correlated to the heat transport convergence in late fall (Fig. A5), but no relation to the probability of MHWs is found (not shown). There is no significant correlation to the AMV. Because the AMV is based on 10-year low-pass filtered temperature timeseries, it is not expected to explain variability on seasonal timescale (Fig. A5).

Therefore, especially the NAO and EAP are linked to heat content changes, but their state does not significantly change the chances of MHW occurrence in most seasons. As argued above for individual MHW events, the initial temperature is also important on seasonal timescales. The initial temperature is defined here as the mean temperature anomaly of the month prior to the season to avoid a large impact of occasionally occurring MHWs that extend across seasons. In most seasons the probability for MHWs is significantly higher, if the month prior to the season was anomalously warm (Fig. 7d). In summer MHWs occur slightly more often without an anomalously warm initial temperature, which causes the p-value to be just above the significance threshold ($p\text{-value} = 0.06$). As will be discussed in more detail below, season mean temperature and initial temperature are closely related, especially in MJJ. Still, there are years in which the season mean temperature anomaly is high, but the initial temperature is neutral or low. The significant dependency for the season mean temperature (Fig. 7a), but non-significant dependency for the initial temperature (Fig. 7d) in MJJ reflects that in these particular years MHWs have occurred (applies to 4 years). This is reasonable because years that had a below average initial temperature anomaly, but still a higher season mean temperature anomaly were likely years with exceptionally strong surface heat flux forcing that also triggered MHWs.

Since the season mean temperature anomaly strongly influences the occurrence of MHWs, we now investigate what drives anomalously warm seasons.

In all seasons except winter, the initial conditions show a higher correlation with the season mean temperature anomaly than the prevailing weather patterns (pressure and climate indices). The correlation is significant with values exceeding 0.43 ($p \ll 0.05$). Especially in summer, the initial temperature has a strong impact and the correlation exceeds 0.8 (Fig. 8e–h).

Linear combinations of the EAP and NAO (and ENSO for late fall) yield a significant correlation to the season mean temperature anomaly only in winter and late fall (Fig. 8e–h). Instead of using climate indices, it is also possible to define a pressure index that directly reflects the local atmospheric conditions over the North Sea. The pressure indices were defined to maximize their correlation to the heat content change during the respective seasons. Only in summer this leads to a higher correlation to the season mean temperature compared to the EAP and NAO (Fig. 8e–h).

When the climate or pressure indices are linearly combined with the initial temperature anomaly, correlations exceed 0.66 ($p \ll 0.05$) in all seasons, except in early fall. The corresponding timeseries are shown in Fig. 8a–d. In early fall the correlation is lower (0.61; $p \ll 0.05$) because neither the established climate indices nor the local pressure index are significantly correlated to the season mean temperature anomaly (Fig. 8g). This suggests that a warm fall can be driven by various weather patterns. Either by shortwave radiation (as in summer), latent heat fluxes, or oceanic heat transport (as in late fall). This is not well captured by the season mean climate or pressure indices. Removing the month of August or October from the group does not improve the performance of the linear model (not shown), which further suggests that the transition between the dominant driver of heat content changes can vary from year to year.

6.2 Variability on longer timescales

The dependency of the seasonal temperature anomalies and occurrence of MHWs on the initial temperature gives rise to variability on longer than seasonal timescales, even without low-frequency variability in the forcing itself and very different mechanisms that govern the temperature evolution in different seasons. Four example periods are selected to illustrate this. We analyze the heat budget for the entire water column here, such that vertical redistribution of heat does not play a role (see methods section for details on the heat budget calculation).

In 1987, the German Bight is in a cold state until it strongly gains heat in late fall by a heat transport convergence, which is followed by a strong surface heat flux anomaly (Fig. 9a). The heat content anomaly reaches a peak in winter 1987/88 resulting in a long-lasting MHW. A large amount of heat is lost again in spring 1988, until the atmosphere drives another strong increase in ocean heat content and multiple MHWs at the beginning of 1989.

In spring 1996, the OHC is strongly negative in the German Bight (Fig. 9b). Until 1998, the heat content gradually increases due to positive surface heat flux anomalies in summer and positive heat transport anomalies in winter. In fall 1997, two MHWs are triggered and several more MHWs occur after a further increase in OHC in 1998.

In winter 2010/11 a strong minimum was reached due to a strongly negative surface heat flux and heat transport anomalies. The recovery from the minimum was initiated in January 2011 by anomalous heat gain from the atmosphere (Fig. 9c). The heat content change was large, but due to the cold initial state it did not lead to any MHWs. Afterwards the heat content remained stable due to offsetting heat transport and surface flux anomalies. After reaching another local minimum, a strong heat gain set in during May 2013. The increase in OHC was first driven by the atmosphere, before anomalous oceanic heat convergence took over. A maximum in heat con-

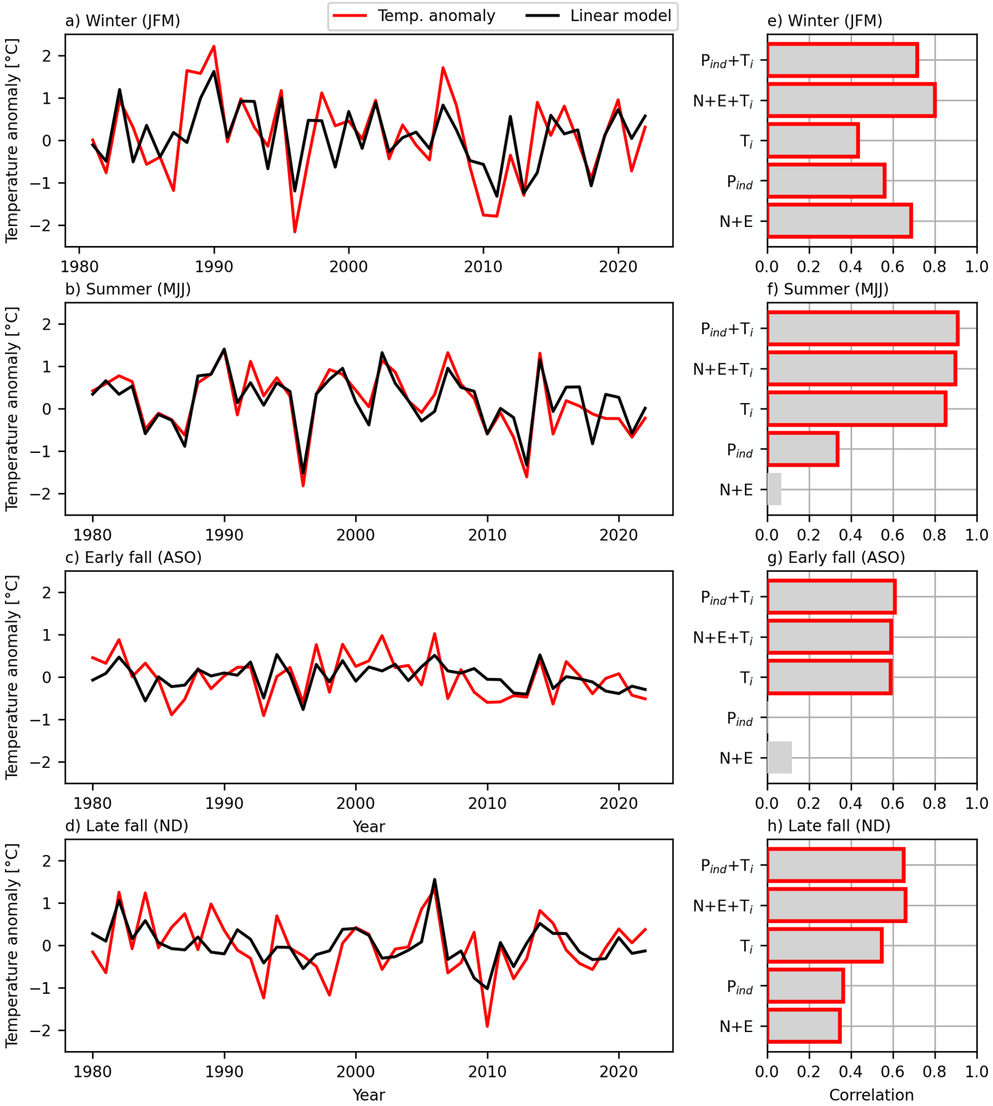

Figure 8. Timeseries of the season mean temperature anomaly in the German Bight and a linear model prediction based on the initial temperature (10 d prior to season start) and a season mean pressure index that reflects the net heat content change **(a–d)**. Correlation coefficients between the season mean temperature anomaly and different input variables **(e–h)**. N+E – linear combination of NAO and EAP index; P_{ind} – local pressure index; T_{i} – initial temperature.

tent that coincided with multiple MHW events was reached in spring 2014.

The most recent years (2019–2023) are characterized by little variability in OHC (Fig. 9d), consistent with the reduced standard deviation of temperature anomalies shown before (Fig. 3). In particular, the surface heat flux anomalies are small. Ocean heat transport anomalies are similar in magnitude compared to other periods, but often compensated by negative surface heat flux anomalies. Only in fall 2022 and 2023 does a strong ocean heat transport anomaly, together with a weakly positive surface heat flux anomaly, increase the ocean heat content and lead to short MHWs. Surface heat flux and heat transport anomalies frequently change sign, such that there is no gradual build-up of heat over multiple seasons either. Instead, the OHC fluctuates around the mean (anomaly of zero) on shorter timescales.

The examples clearly illustrate how the history of surface heat flux and heat transport anomalies influence the heat content of the German Bight and contributes to preconditioning for MHWs over multiple seasons. A peak in ocean heat content on interannual to pentadal timescales may be reached by a strong heating anomaly during a single season (e.g. winter 1987/88), that is maintained in the following seasons. In other periods, however, a peak in OHC results from a more gradual build up of heat anomalies over multiple seasons within a year (e.g. May 2013 to April 2014) or over multi-

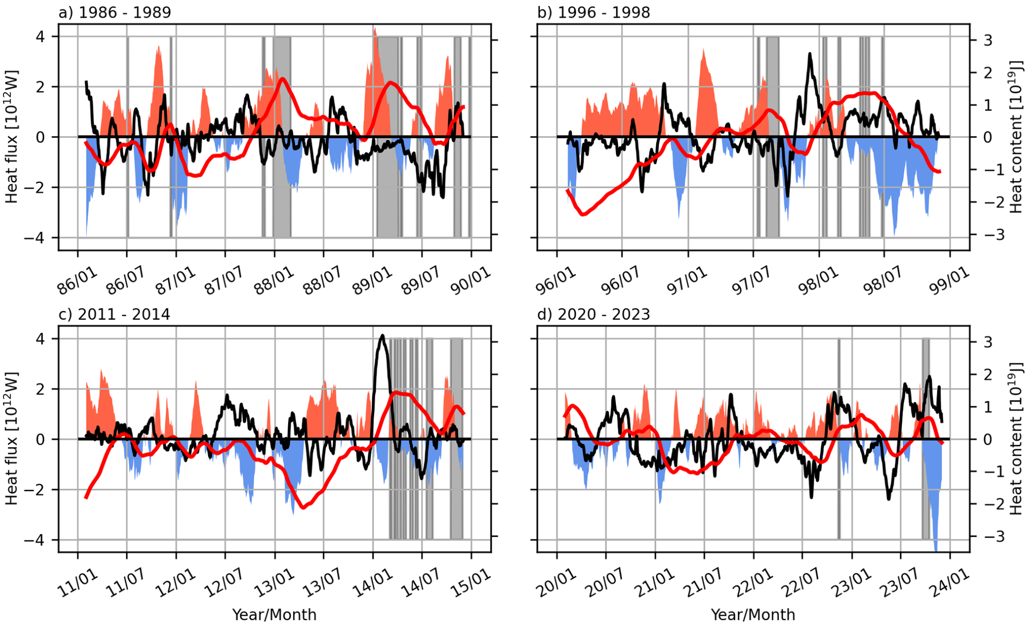

Figure 9. Heat budget for the German Bight during four selected time periods. The heat content anomaly (red; relative to the detrended baseline) is shown along with the net ocean heat transport (black) and net surface heat flux (shading) anomalies. Grey shading indicate MHWs (detrended baseline) in the German Bight.

ple years (e.g. from March 1996 to July 1998). Often MHWs follow periods of sustained positive surface heat flux anomalies in summer and positive heat transport anomalies in the following winter (e.g. 1996–1998 or 2013–2014). Therefore, it is usually not the conditions (e.g. NAO/EAP) in a single season that matter for the occurrence of MHWs, but the prevailing (and cumulating) atmospheric conditions over multiple seasons.

7 Local and remote forcing of German Bight MHWs

On interannual timescales, there is a strong anti-correlation of the surface heat flux and heat transport convergence in the German Bight (-0.8; $p \ll 0.05$; Fig. 10a). A warming driven by oceanic heat convergence increases the latent, sensible and longwave heat loss to the atmosphere. Conversely, a local heat flux warming leads to a higher temperature of the outflow of the German Bight, which reduces the heat convergence. Significant anti-correlations are found between heat convergence and sensible heat flux (-0.5; $p < 0.05$), but not for the other components (-0.13 to -0.3 with $p > 0.05$). This suggests that weather patterns that lead to a stronger heat convergence are often associated with reduced surface heat fluxes, but not always the same heat flux component is affected. For example such a weather pattern could be either associated with more dry air advection (more evaporative cooling) or more cloud cover (less shortwave heating).

Strong changes in OHC therefore result from unbalanced surface heat flux and heat convergence anomalies, rather than strong anomalies in only one of the components. This is supported by the relatively small (< 0.4) correlation between the OHC change and the two fluxes, which is only significant for the surface heat flux.

A more detailed analysis of heat transport convergence in the German Bight reveals that changes can be driven by both changes in heat transport across the northern ($R = 0.6$, $p \ll 0.05$) or western boundary ($R = 0.7$, $p \ll 0.05$; Fig. 10b). The correlation between the two transports themselves is close to zero (-0.02; $p \gg 0.05$). While the western boundary transport is closely related to the heat transport through the English Channel ($R = 0.66$; $p \ll 0.05$), the transport across the northern boundary of the North Sea (between Scotland and Norway) does not seem to affect the heat transport into the German Bight.

To gain more insight into how the important inflow through the English Channel is related to variability outside the North Sea, we split the heat transport into the contribution of velocity and temperature anomalies. Here we use a volume integrated temperature in the southwestern North Sea as the reference temperature to ensure that changes in the heat transport are associated with a local warming/cooling.

The most important contribution to changes of the heat transport comes from circulation anomalies that act on the mean temperature ($u'\overline{T}$; Fig. 10c). It shows the largest standard deviation (1.4×10^{11} W) and highest correlation (0.83, $p < 0.05$) to the total heat transport. A stronger inflow leads to a warming of the southwestern North Sea, because the mean temperature of Atlantic water is higher than the mean local temperature. Changes in the temperature of the inflow itself ($\overline{u}T'$) are important as well. They are highly correlated

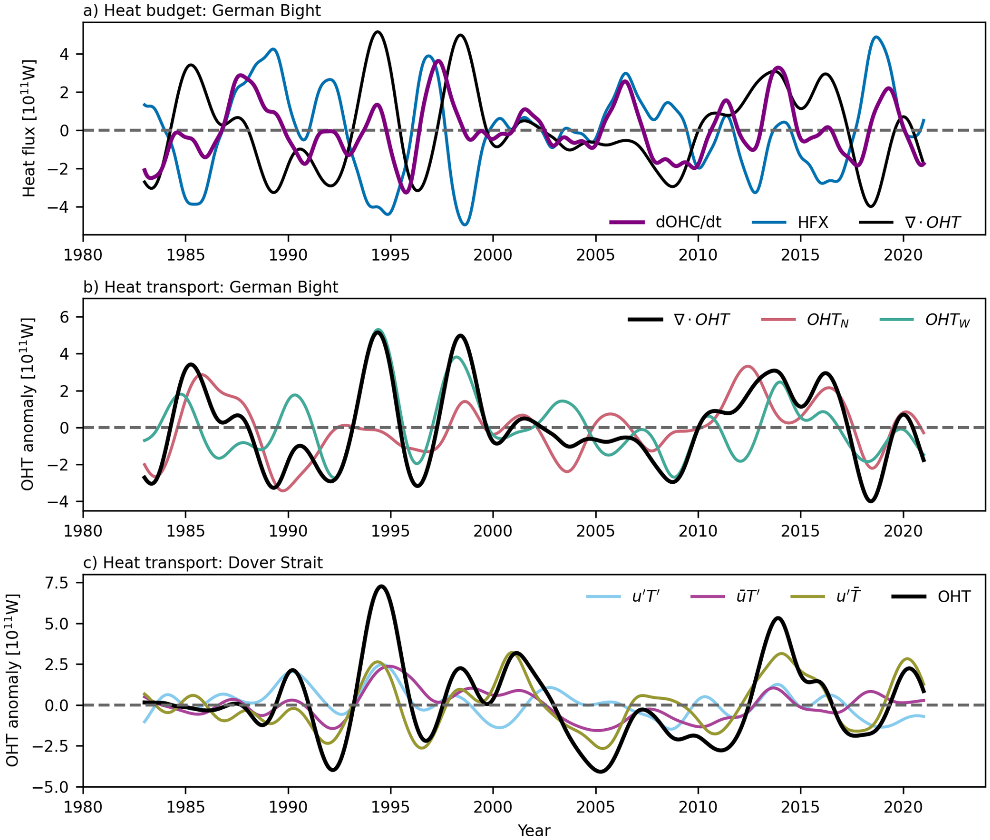

Figure 10. Heat Budget of the German Bight **(a)**. The heat content change is decomposed into the contribution of the ocean heat transport (OHT) divergence and surface heat flux (HFX). The heat transport is further decomposed into the contribution of the northern ($\mathrm{OHT_N}$) and western ($\mathrm{OHT_W}$) boundary transports **(b)**. Anomalies of the heat transport through the English Channel at Dover Strait **(c)** are split into the contribution of the mean temperature/transport ($\overline{T}/\overline{u}$) and temperature/transport anomalies (T'/u').

to the total heat transport (0.79, $p < 0.05$), but less variable than the circulation contribution (0.84×10^{11} W) (Fig. 10c). The covariance term ($u'T'$) shows the lowest correlation to the total heat transport (0.54, $p < 0.05$).

The strength and temperature of the inflow into the North Sea influences the heat content (temperature) of the German Bight and thus the occurrence of MHWs. To further test the impact of remote ocean temperature variability, we ran a model experiment where the heat flux inside and outside the North Sea are derived from different decades. In our forced simulation, the North Sea SST is surprisingly insensitive to the conditions outside the North Sea and almost all of the variability is explained by the local atmospheric conditions. This is especially true for the German Bight. East of 5° E, temperature differences between the sensitivity and reference experiments are near zero (Fig. 11a).

Although temperature anomalies exceed 2 °C at the Atlantic entrance of the English Channel, the heat transport is nearly indistinguishable between the two experiments already in the central English Channel (Fig. 11a, b). Although temperature anomalies influence the heat transport across Dover Strait, temperature anomalies are strongly damped by the surface heat flux before they reach Dover Strait (Fig. 11a). The heat flux and SST anomalies are highly anticorrelated in the transition zone between the interior and exterior of the North Sea (between the dashed lines in Fig. 11a), such that a higher temperature results in a stronger heat loss to the atmosphere. The most important component that results in this damping effect is the latent heat flux (Fig. 11c). A higher/lower SST leads to a higher/lower saturation pressure at the sea surface and increased/decreased evaporation. The volume transport seems to be mostly driven by the local wind stress that is the same in both experiments. The temperature gradient between the Atlantic and North Sea does not influence the volume transport. As a consequence, the oceanic heat transport into the North Sea is not distinguishable from the reference experiment and because the local surface heat flux is (almost) the same by construction, the German Bight temperature remains the same. It should be mentioned that this does not mean the temperature of the North Sea is independent of the oceanic conditions outside the North Sea. Rather, it suggests that changes in the Atlantic affect the North Sea via coupled ocean-atmosphere changes. This is discussed in more detail in the discussion section.

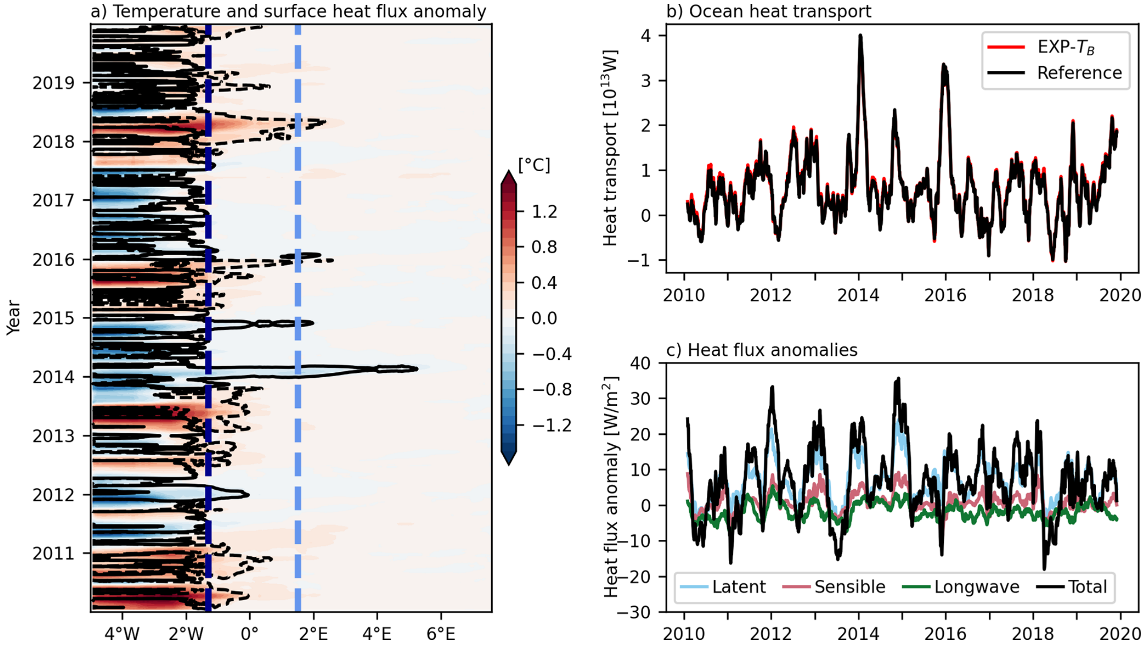

Figure 11. Hovmöller diagram of the surface temperature anomaly (sensitivity – reference) and surface heat flux anomaly in the southern North Sea **(a)**. The dark blue line indicates the end of the transition zone between the different heat flux forcings and the light blue line indicates Dover Strait. Ocean heat transport across the dark blue line (central English Channel; **b**) and heat flux anomalies in the area between the dark and light blue lines **(c)**.

8 Summary and Discussion

8.1 Recent changes of MHWs in the southern North Sea

The North Sea experienced a strong warming in the late 1980s and has continued to warm (at a lower rate) afterwards (Meyer et al., 2011; Mohamed et al., 2025). This temporal evolution is well represented by a number of satellite, reanalysis and model-based datasets, such as VIKING20X. Along with the long-term warming, MHWs became more frequent in the North Sea relative to a fixed baseline, consistent with previous studies (Mohamed et al., 2023, 2025; Lin et al., 2025; Giménez et al., 2024). Due to large interannual variability, only trends in frequency are significant in most, but not all, datasets when the overlap period of all datasets is considered (1993–2023). The duration and number of MHW days have increased, but the linear trends are not statistically significant in most datasets. When the full satellite period (1982–2023) is considered in datasets that cover this period, trends in frequency, duration, and MHW days are significantly different from zero for most of them. In contrast, the maximum intensity has not increased. For both the overlap and the full satellite period trends in maximum intensity are not significantly different from zero (and tend to be negative) in any dataset. While interannual variability shows very high agreement between different satellite and model-based datasets with correlations exceeding 0.8, linear trends can differ. Such a result was also obtained for the Indo-Pacific region (Zhang et al., 2024). Especially the OIS dataset shows stronger trends in the temperature and MHW characteristics than other datasets in the North Sea. This is an important result, because the OIS dataset is used for example by Mohamed et al. (2025) as the only dataset to assess past trends in North Sea MHWs. Although we don't expect their results to fundamentally change with other datasets, their trend estimates are likely at the upper limit. As expected, the variability in the reanalysis datasets, that both assimilate the OST surface temperatures in this case, is very similar. Still, trends show slightly different patterns and lower values, suggesting that the model choices play a role too. Simulations with the forced ocean model VIKING20X that does not assimilate ocean observations shows a very similar temporal evolution (variability and trends).

In agreement with Mohamed et al. (2025), the increase in MHW frequency is largely caused by the linear temperature trend. Relative to a detrended baseline we find no linear increase in the MHW characteristics in any of the datasets. Especially the years after 2019 showed only few MHWs. This suggests that natural sub-decadal variability has damped the effects of the long-term trend in recent years.

8.2 Drivers and vertical structure of MHWs in the German Bight

In line with previous studies, MHWs in late spring and summer are usually driven by increased shortwave radiation and reduced vertical mixing in the ocean, associated with a high pressure system over Scandinavia (Mohamed et al., 2025; Berthou et al., 2024). A somewhat similar weather pattern can lead to MHWs driven by anomalous latent heat flux that typically occurs in late summer/early fall. Most winter MHWs are driven by the ocean heat transport and associated with a very different weather pattern. A low-pressure system located northeast of Scotland and strong south-westerly winds over the English Channel drive a large amount of warm Atlantic water into the southern North Sea.

Consistent with the drivers of MHWs, they have different vertical structure. Shortwave driven MHWs occur in the top few meters of the ocean with much smaller anomalies below. This is consistent with a case study by Berthou et al. (2024) and a decoupling of SST anomalies and vertically integrated OHC in summer (Pohlmann, 1996). Chen et al. (2022) argue that MHWs themselves are an important driver of stratification in the shallow southern North Sea that is usually well mixed by tides and wind/wave induced mixing. This has important consequences, since many mobile marine species may be able to avoid the high surface temperatures and benthic species are only affected in very shallow regions close to the coast. For the German Bight, these regions are mostly tidal flats and experience much larger variability caused by a regular exposure to the air temperature. Due to the strong temperature gradient near the surface, models with coarse vertical resolution and no data assimilation (V20 and CST1) underestimate the intensity of MHWs. They simulate a mean temperature of the surface layer (here 5–6 m thick), which is not representative for the temperature in the top meter during summer MHWs. In contrast, the BSH model, which does not use data assimilation either, shows maximum temperature anomalies much more comparable to the satellite-based datasets. The presence (CST1 & BSH) or absence (V20) of tidal mixing seems to be less important than the vertical resolution (and potentially vertical mixing parameterizations). Similarly, latent heat driven MHWs show stronger anomalies at the surface, but the vertical temperature gradient is smaller compared to SW-driven MHWs. MHWs in winter are often driven by ocean heat transport anomalies under strong winds and therefore the water column is well mixed in the German Bight. There are no substantial biases between the datasets for these MHWs, resulting in an almost flat seasonal cycle of MHW intensity in V20, whereas satellite measurements show pronounced seasonal cycles.

8.3 Interaction of timescales and ocean preconditioning

While MHWs are associated with distinct atmospheric patterns they are not a sufficient condition for MHWs to occur. Even exceptionally strong atmospheric anomalies that are associated with strong heat flux (i.e. heat content change) anomalies do not necessarily result in MHWs. The reason for this result is that the temperature and equivalently the ocean heat content are integrated properties. A given (surface or lateral) heat flux changes the temperature, but whether the temperature is anomalously high (i.e. a MHW occurs) depends on the history of the fluxes. Weather related variability on timescales of days to weeks is strongly linked to the fluxes (e.g. solar insolation, stronger heat transport), that is changes in temperature, but not absolute temperature anomalies. Therefore, processes that lead to a warming of the ocean on longer, seasonal to decadal, timescales (ocean preconditioning) play a major role for the occurrence of MHWs.

With the detrended baseline, this ocean preconditioning is related to seasonal to decadal variability. With the fixed baseline, the long-term warming trend acts as an additional preconditioning factor. Which timescales contribute to the trend versus variability relative to the trend depends on the chosen period for detrending and analysis. In this study, the period is 1993 to 2022 (30 years) and thus multidecadal variability (e.g. the AMV) contributes mostly to the trend, while variability on interannual timescales (e.g. NAO) mostly contributes to variability relative to the trend. Therefore, the long-term trend itself probably contains anthropogenic forcing, but also low-frequency natural variability. The AMV index has increased from the mid 90s up to now, which is exactly the same time period of the linear trend in our and most other MHWs studies in the North Sea (e.g. Mohamed et al., 2025). It is also interesting to note that temperature is often assumed to show larger variability on longer timescales (red spectrum; Frankignoul and Hasselmann, 1977). Therefore, the longest timescale covered by a timeseries is expected to dominate the occurrence of MHWs.

On seasonal timescales the occurrence of MHWs is linked to the prevailing weather conditions during the season, but more importantly to the initial temperature (i.e. the temperature evolution in the prior season). Especially the summer mean temperature anomaly is almost entirely explained by the temperature in late winter/ spring. This is consistent with Mathis et al. (2015) and Pohlmann (1996), who found the summer temperature to be highly correlated with the atmospheric conditions and SST in previous seasons. A reason for this observation is a strong anti-correlation between different heat flux components and with the ocean heat transport. A summer with strong solar insolation is often accompanied by more heat loss through the transport and/or the other surface heat flux components. A similar damping mechanism was already observed by Elliott and Clarke (1991) in an idealised 2-layer model of the North Sea.

Consistent with the view that temperature is an integrated quantity (i.e. it is set by temporally integrated fluxes) and climate indices being more related to temperature changes than absolute temperature anomalies, we only find a statistically significant dependency of MHWs on the state of the EAP in winter. For other climate indices previously found to be important (Lin et al., 2025; Mohamed et al., 2023, 2025), such a dependency was not found. For the AMV this is likely explained by the fact that Mohamed et al. (2023, 2025) used a fixed baseline. As mentioned above the AMV showed an almost linear increase from the mid 1990s to 2020s and therefore aligns with the temperature trend in the North Sea. Here we used a detrended baseline to explain the natural variability contribution on interannual to decadal timescales. In agreement with Lin et al. (2025) we find the NAO to be strongly related to the surface heat flux in winter and the EAP to the inflow of warm water through the English Channel. The NAO is not related to the heat transport in the southern North Sea in most seasons (including winter), which was also noted by Hjøllo et al. (2009) and Mathis et al. (2015). Thus a link between NAO/EAP and MHWs exists, but the NAO and EAP being positive is not a sufficient condition for MHWs to occur. The temperature anomaly at the beginning of the seasons is more important in most seasons, except for the winter months (JFM).

The strong impact of the season's initial temperature gives rise to the strong impact of low-frequency variability. The North Sea can build up heat over several seasons or even several years. More detailed analysis based on the model output shows that the surface heat flux and oceanic heat convergence both contribute to heat content changes. As most of the climate indices do not have the same influence year round, a positive NAO winter is associated with a warming North Sea in winter, which is not necessarily the case for a positive NAO year. In summer for example, a positive NAO state is correlated to a stronger surface heat flux, but the effect is compensated by a negative correlation to the oceanic heat transport convergence. Therefore, also on longer timescales a single climate index can not explain the evolution of the German Bight's temperature. It is rather a series of positive NAO/EAP winters that leads to a warm state of the southern North Sea.

8.4 The impact of remote variability

The inflow of warm water through the English Channel has a strong influence on the southern North Sea and MHWs in the German Bight, consistent with Chen et al. (2022) and Mathis et al. (2015). Especially variations in transport are important, but variations in the inflow temperature also play a role. Still, our sensitivity experiments suggest that SST in the North Sea (especially in the German Bight) is almost fully determined by the atmospheric state on decadal and shorter timescales, consistent with results obtained by Meyer et al. (2011) and Giménez et al. (2024). The reason for this result is that the transport is largely driven by the local winds over the English Channel (Mathis et al., 2015) and the temperature of the inflow is set by the local surface heat flux (Taylor and Stephens, 1983). Even strong temperature anomalies in the eastern Atlantic do not enter the North Sea under a prescribed atmospheric state, because they are quickly damped by the surface heat flux.

Nevertheless, our forced ocean model experiments are not able to answer the question how remote changes that are for example related to the large-scale Atlantic circulation feed back on the local atmospheric state in the North Sea. In reality a changing surface temperature in the eastern Atlantic affects the surface heat fluxes that, in contrast to our simulations, change the atmospheric conditions. Therefore, it cannot be concluded based our experiments that the temperature outside the North Sea is not important. As noted above, Meyer et al. (2011) find a similarly strong dependency of the German Bight's temperature on the local atmospheric conditions, but they use a forced ocean model as well. Whether variability of the Atlantic Ocean circulation, for example, is linked to temperature variability in the North Sea therefore remains to be studied in a coupled model set-up.

This result has several implications. Forced simulations are very useful if the goal is to understand the past evolution of MHWs with physically consistent ocean and atmosphere states. That the temperature evolution is strongly determined by the atmospheric state is very useful for regional models, because not simulating interannual variability outside the North Sea does not introduce errors in the central and southern North Sea. The strong dependency on the atmospheric state is consistent with all model datasets showing a very similar evolution of MHWs, despite very different set-ups. Furthermore, atmospheric observations are readily available and contain a lot of information about the ocean's temperature. With an accurate initial ocean state, predictions of the pressure field would allow for potential predictability of MHWs. Given that Krieger et al. (2025, 2022) have shown that skillful predictions of local atmospheric variables are possible, this could also allow the prediction of MHW likelihood. Note that on seasonal timescales the initial state already contains a lot of information on the likelihood of MHWs.

Nevertheless, when the goal is to understand the full physical mechanisms involved in the evolution of MHWs, i.e. the initial source of temperature anomalies, coupled model experiments are required. The large-scale oceanic circulation could play an important role in shaping the atmospheric state over the North Sea, such that the evolution of MHWs could be strongly, but indirectly, influenced by remote oceanic variability.

9 Conclusions

Marine heatwaves have become more frequent and longer, but less intense in the German Bight over the recent decades relative to a fixed baseline. Different datasets agree on the sign of the trends, but not statistical significance. When a detrended baseline is used, the impact of pentadal to decadal variability in the North Sea's temperature is emphasized, which was in a neutral to low phase after 2018. Given that temperature is an integrated property, the reason is not just related to the occurrence of specific weather patterns, but rather results from the interaction of variability on different timescales. Seasonal variability in the heat fluxes was small after 2018 and variability in the ocean heat transport convergence was often balanced by the surface heat flux. Therefore, there was neither a strong warming on seasonal timescales, nor a continuous warming over multiple seasons that could have led to many/strong MHWs. This is connected to a relatively low standard deviation of temperature anomalies and thus fewer extremes. The fixed baseline results which contain both the long-term warming trend and variability on shorter timescales show an increase in frequency and duration driven by the trend, but a slight reduction in intensity due to the lower standard deviation of temperature anomalies. The future evolution of MHWs will depend on whether the long-term warming trend continues and the phase of shorter-timescales variability. The former is not certain on decadal and shorter timescales, because on these timescales the trend is a mix of anthropogenic forcing and natural variability (e.g. related to the AMV). Furthermore, our results suggest that variability of the North Sea's temperature is dominated by the local atmospheric conditions over the Northwest European Shelf. How these atmospheric conditions, in turn, are linked to oceanic variability in the North Atlantic remains to be studied.

Appendix A: Additional figures

A1 Mean seasonal cycle

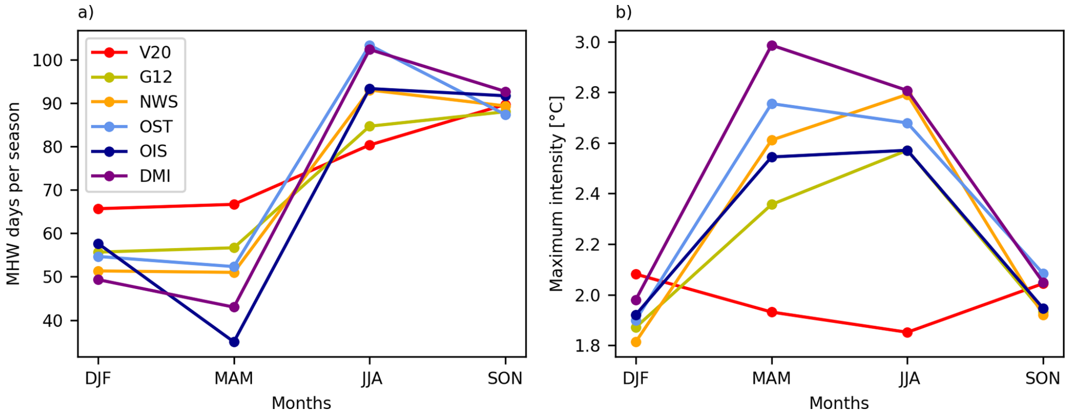

Figure A1. Mean seasonal cycle in different datasets. Number of marine heatwaves days per season **(a)** and mean maximum intensity of heatwaves in the seasons **(b)**.

A2 Vertical temperature profiles

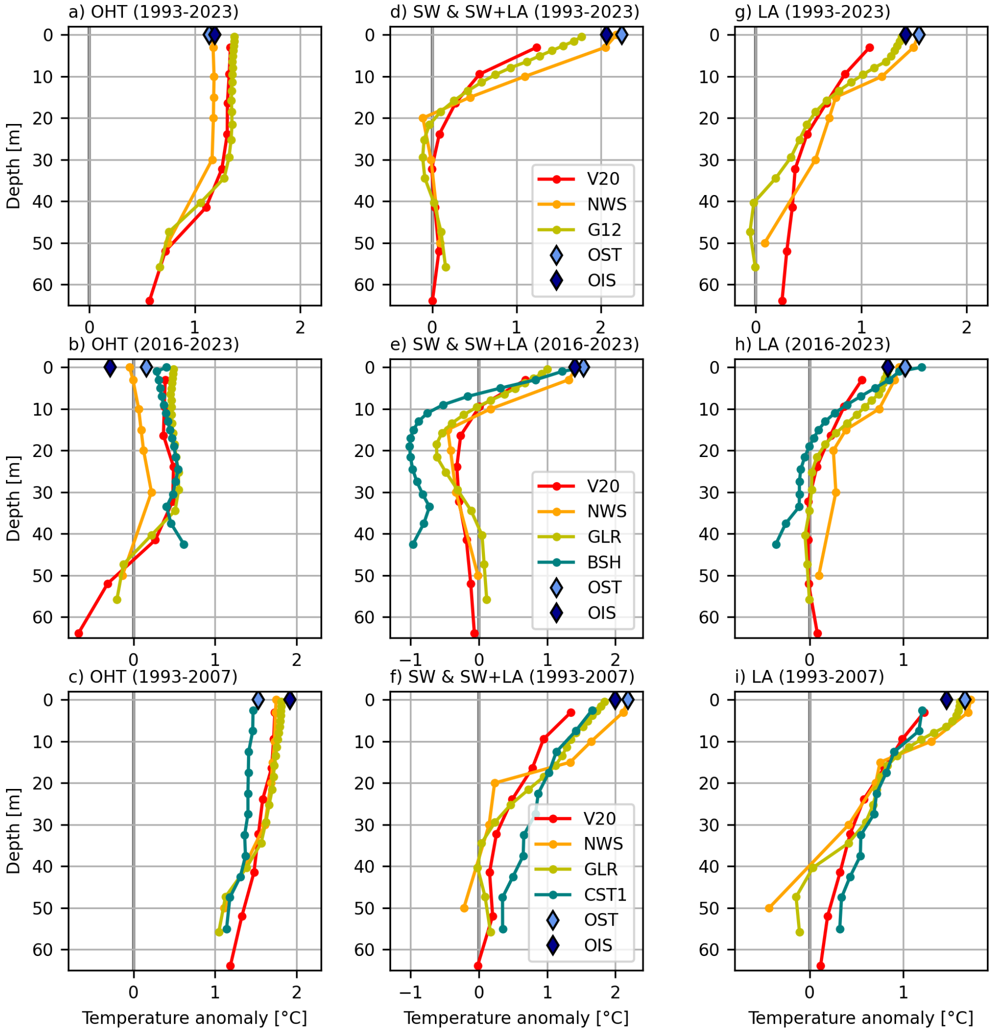

Figure A2. Mean temperature anomaly during all MHWs driven by ocean heat transport anomalies **(a–c)**, shortwave and latent heat flux anomalies **(d–f)** and latent heat flux anomalies only **(g–i)**. Start and end date of MHWs were taken from VIKING20X for all datasets, such that the mean is derived for the same days for all datasets. The fixed 30-year baseline (1993–2022) is used as a reference in a,d,g and a shorter baselines (2016–2023/1993–2007) in panels **(d)**–**(f)**/**(g)**–**(i)** for comparison with the BSH/CST1 datasets. For all panels only MHW events that occurred within the respective baseline period are considered.

A3 Composites for detrended baseline MHWs

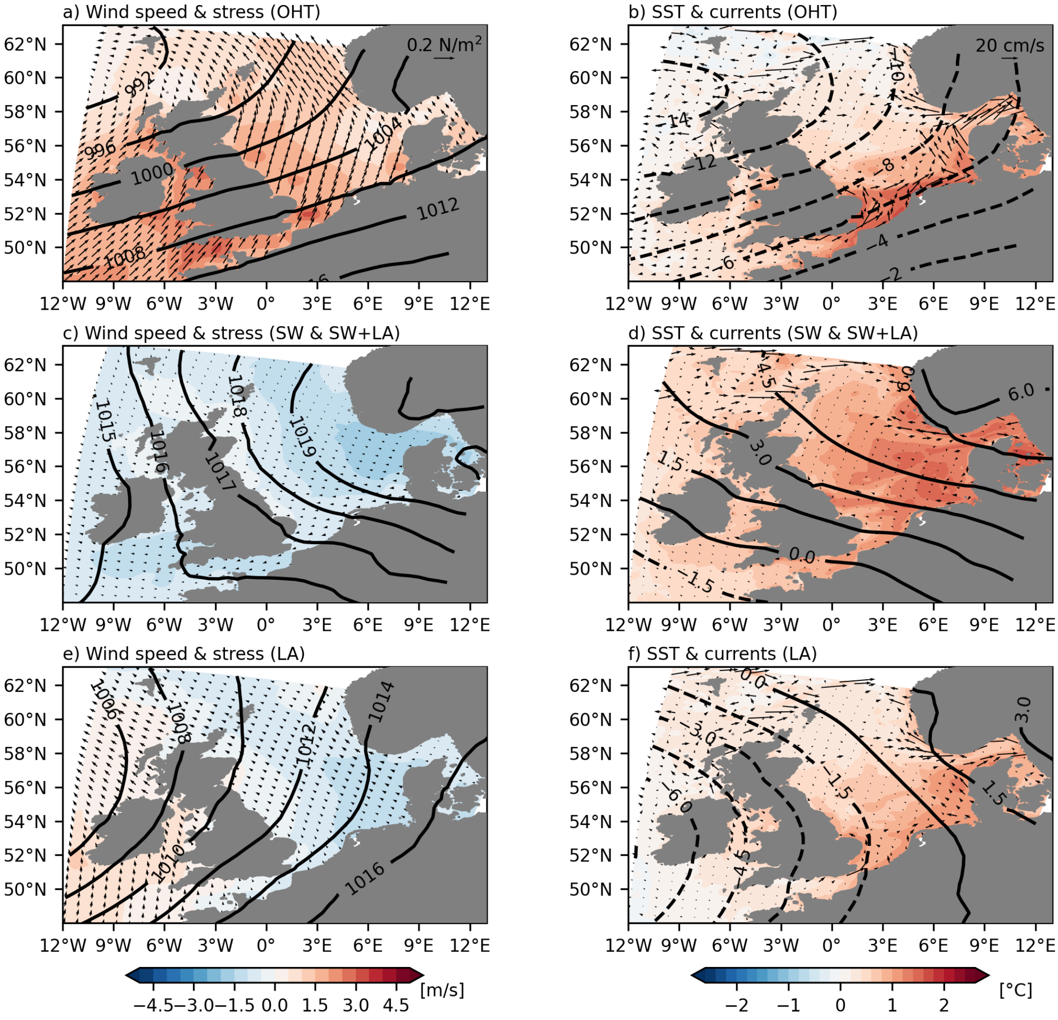

Figure A3. Mean oceanic and atmospheric conditions during the onset of MHWs (detrended baseline) driven by the ocean heat transport **(a, b)**, shortwave or shortwave and latent heat flux **(c, d)** and latent heat flux alone **(e, f)**. All maps show the composite of all MHWs that were attributed to the mentioned drivers (see methods for details). Contours show the air pressure in hPa **(a, c, e)** or the air pressure anomaly **(b, d, f)**. Arrows show the wind stress anomaly **(a, c, e)** and surface current anomaly **(b, d, f)**. Shading shows the wind speed anomaly **(a, c, e)** and sea surface temperature anomaly **(b, d, f)**.

A4 English Channel inflow anomalies

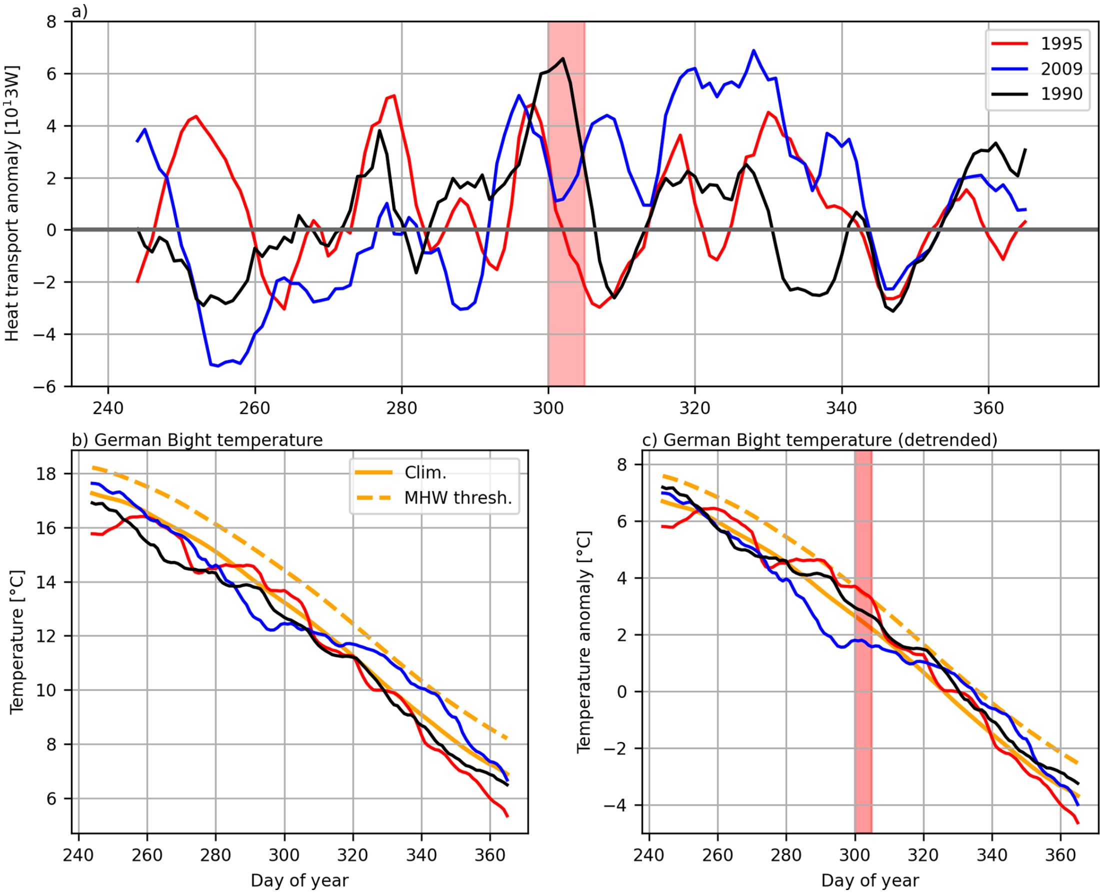

Figure A4. Heat transport anomaly through the English Channel (Dover Strait) in autumn of three selected years **(a)**. Red shading indicates MHW days in the German Bight in 1995 (in 2009 and 1990 no MHW days have occurred; detrended baseline). The temperature **(b)** and detrended temperature **(c)** for the same years are shown along with the respective climatologies and MHW thresholds for the fixed and detrended baselines.

A5 Correlation to climate indices

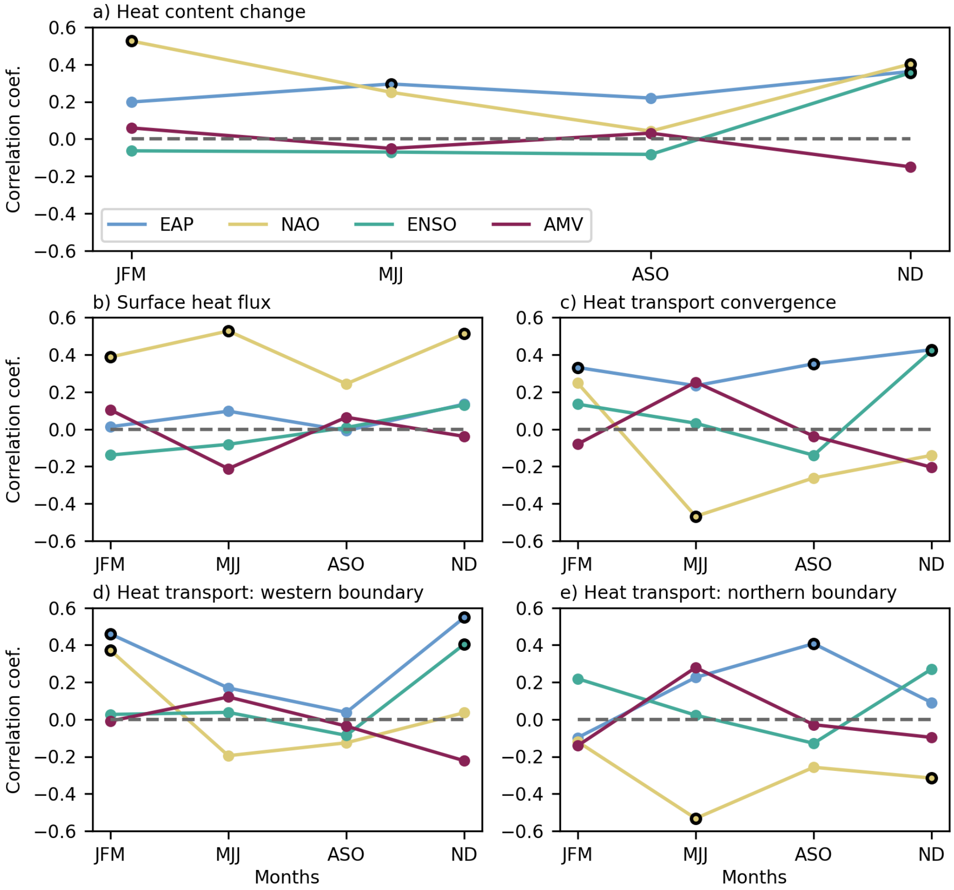

Figure A5. Correlation of heat budget terms with different climate indices for each season. Abbreviations on the x-axis indicate the months. Statistically significant correlation coefficients based on a 5 % significance level are indicated by black circles.

Code and data availability. The full 4-dimensional model output (North Sea region) of our main experiment VIKING20X-KTS001 is available through https://hdl.handle.net/20.500.12085/f2d595cc-10c7-11f1-a464-005056a30ade (Schulzki et al., 2026a). Additional derived output shown in this publication, data from the sensitivity experiments and the scripts used to generate the derived output and figures is available from https://hdl.handle.net/20.500.12085/6dd5ffce-10c7-11f1-a1b6-005056a30ade (Schulzki et al., 2026b). All model and observation based datasets used here in addition to our own model experiments are freely available. The sources are referenced in the data section.

Author contributions. AB initiated and designed the study. TS performed the numerical model experiments, with support from FUS. All authors contributed to the design of the analysis, which TS performed. TS wrote the paper draft, which all authors jointly iterated.

Competing interests. The contact author has declared that none of the authors has any competing interests.

Acknowledgements. The authors gratefully acknowledge the Earth System Modelling Project (ESM) for funding this work by providing computing time on the ESM partition of the supercomputer JUWELS at the Juelich Supercomputing center (JSC).

Financial support. The study was supported by the Federal Ministry of Research, Technology and Space (BMFTR) through the project METAscales (grant no. 03F0955J), as well as the northern German states within the scope of the German Marine Research Alliance (DAM) mission mareXtreme.

The article processing charges for this open-access
publication were covered by the GEOMAR Helmholtz Centre
for Ocean Research Kiel.

Review statement. This paper was edited by Karen J. Heywood and reviewed by Segolene Berthou and one anonymous referee.

References

Amaya, D., Jacox, M., Fewings, M., Saba, V., Stuecker, M., Rykaczewski, R., Ross, A., Stock, C., Capotondi, A., Petrik, C., Bograd, S., Alexander, M., Cheng, W., Hermann, A., Kearney, K., and Powell, B.: Marine heatwaves need clear definitions so coastal communities can adapt, Nature, 616, 29–32, https://doi.org/10.1038/d41586-023-00924-2, 2023.

Arias-Ortiz, A., Serrano, O., Masqué, P., Lavery, P. S., Mueller, U., Kendrick, G. A., Rozaimi, M., Esteban, A., Fourqurean, J. W., Marbà, N., Mateo, M. A., Murray, K., Rule, M. J., and Duarte, C. M.: A marine heatwave drives massive losses from the world's largest seagrass carbon stocks, Nat. Clim. Change, 8, 338–344, https://doi.org/10.1038/s41558-018-0096-y, 2018.

Berthou, S., Renshaw, R., Smyth, T., Tinker, J., Grist, J. P., Wihsgott, J. U., Jones, S., Inall, M., Nolan, G., Berx, B., Arnold, A., Blunn, L. P., Castillo, J. M., Cotterill, D., Daly, E., Dow, G., Gómez, B., Fraser-Leonhardt, V., Hirschi, J. J.-M., Lewis, H. W., Mahmood, S., and Worsfold, M.: Exceptional atmospheric conditions in June 2023 generated a northwest European marine heatwave which contributed to breaking land temperature records, Commun. Earth Environ., 5, 287, https://doi.org/10.1038/s43247-024-01413-8, 2024.

Biastoch, A., Schwarzkopf, F. U., Getzlaff, K., Rühs, S., Martin, T., Scheinert, M., Schulzki, T., Handmann, P., Hummels, R., and Böning, C. W.: Regional imprints of changes in the Atlantic Meridional Overturning Circulation in the eddy-rich ocean model VIKING20X, Ocean Sci., 17, 1177–1211, https://doi.org/10.5194/os-17-1177-2021, 2021.

Blanke, B. and Delecluse, P.: Variability of the Tropical Atlantic Ocean Simulated by a General Circulation Model with Two Different Mixed-Layer Physics, J. Phys. Oceanogr., 23, 1363–1388, https://doi.org/10.1175/1520-0485(1993)023<1363:VOTTAO>2.0.CO;2, 1993.

Brüning, T., Janssen, F., Kleine, E., Komo, H., Maßmann, S., Menzenhauer-Schumacher, I., Jandt, S., and Dick, S.: Operational Ocean Forecasting for German Coastal Waters, Die Küste, 81, 273–290, 2014.

Chafik, L., Nilsen, J. E. Ø., and Dangendorf, S.: Impact of North Atlantic Teleconnection Patterns on Northern European Sea Level, Journal of Marine Science and Engineering, 5, https://doi.org/10.3390/jmse5030043, 2017.

Chen, W. and Staneva, J.: Characteristics and trends of marine heatwaves in the northwest European Shelf and the impacts on density stratification, in: 8th edition of the Copernicus Ocean State Report (OSR8), edited by: von Schuckmann, K., Moreira, L., Grégoire, M., Marcos, M., Staneva, J., Brasseur, P., Garric, G., Lionello, P., Karstensen, J., and Neukermans, G., Copernicus Publications, State Planet, 4-osr8, 7, https://doi.org/10.5194/sp-4-osr8-7-2024, 2024.

Chen, W., Schulz-Stellenfleth, J., Grayek, S., and Staneva, J.: Impacts of the Assimilation of Satellite Sea Surface Temperature Data on Volume and Heat Budget Estimates for the North Sea, J. Geophys. Res.-Oceans, 126, e2020JC017059, https://doi.org/10.1029/2020JC017059, 2021.

Chen, W., Staneva, J., Grayek, S., Schulz-Stellenfleth, J., and Greinert, J.: The role of heat wave events in the occurrence and persistence of thermal stratification in the southern North Sea, Nat. Hazards Earth Syst. Sci., 22, 1683–1698, https://doi.org/10.5194/nhess-22-1683-2022, 2022.

Deschamps, M. M., Boersma, M., and Giménez, L.: Responses of the mesozooplankton community to marine heatwaves: Challenges and solutions based on a long-term time series, J. Anim. Ecol., 93, 1524–1540, https://doi.org/10.1111/1365-2656.14165, 2024.

Elliott, A. and Clarke, T.: Seasonal stratification in the northwest European shelf seas, Cont. Shelf Res., 11, 467–492, https://doi.org/10.1016/0278-4343(91)90054-A, 1991.

E.U. Copernicus Marine Service Information (CMEMS): Atlantic-European North West Shelf - Ocean Physics Reanalysis, Marine Data Store (MDS), https://doi.org/10.48670/moi-00059, last access: 21 January 2024a.

E.U. Copernicus Marine Service Information (CMEMS): Baltic Sea - Sea Surface Temperature Reprocessed, Marine Data Store (MDS), https://doi.org/10.48670/moi-00156, last access: 1 November 2024b.

E.U. Copernicus Marine Service Information (CMEMS): Global Ocean OSTIA Sea Surface Temperature and Sea Ice Reprocessed, Marine Data Store (MDS), https://doi.org/10.48670/moi-00168, last access: 11 May 2024c.

E.U. Copernicus Marine Service Information (CMEMS): Global Ocean Physics Reanalysis, Marine Data Store (MDS), https://doi.org/10.48670/moi-00021, last access: 29 October 2024d.

E.U. Copernicus Marine Service Information (CMEMS): Global Ocean OSTIA Sea Surface Temperature and Sea Ice Analysis, Marine Data Store (MDS), https://doi.org/10.48670/moi-00165, last access: 25 October 2025.

Frankignoul, C. and Hasselmann, K.: Stochastic climate models, Part II Application to sea-surface temperature anomalies and thermocline variability, Tellus, 29, 289–305, https://doi.org/10.3402/tellusa.v29i4.11362, 1977.

Garrabou, J., Coma, R., Bensoussan, N., Bally, M., Chevaldonné, P., Cigliano, M., Diaz, D., Harmelin, J. G., Gambi, M. C., Kersting, D. K., Ledoux, J. B., Lejeusne, C., Linares, C., Marschal, C., Pérez, T., Ribes, M., Romano, J. C., Serrano, E., Teixido, N., Torrents, O., Zabala, M., Zuberer, F., and Cerrano, C.: Mass mortality in Northwestern Mediterranean rocky benthic communities: effects of the 2003 heat wave, Glob. Change Biol., 15, 1090–1103, https://doi.org/10.1111/j.1365-2486.2008.01823.x, 2009.

Giménez, L., Boersma, M., and Wiltshire, K. H.: A multiple baseline approach for marine heatwaves, Limnol. Oceanogr., 69, 638–651, https://doi.org/10.1002/lno.12521, 2024.

Good, S., Fiedler, E., Mao, C., Martin, M. J., Maycock, A., Reid, R., Roberts-Jones, J., Searle, T., Waters, J., While, J., and Worsfold, M.: The Current Configuration of the OSTIA System for Operational Production of Foundation Sea Surface Temperature and Ice Concentration Analyses, Remote Sens., 12, https://doi.org/10.3390/rs12040720, 2020.

Großelindemann, H., Ryan, S., Ummenhofer, C. C., Martin, T., and Biastoch, A.: Marine Heatwaves and Their Depth Structures on the Northeast U.S. Continental Shelf, Front. Clim., 4, https://doi.org/10.3389/fclim.2022.857937, 2022.

Helmholtz-Zentrum Geesthacht, Zentrum für Material- und Küstenforschung GmbH (HZG): coastDat-1 HAMSOM baroclinic hydrodynamic hindcast (1948–2007) North Sea, World Data Center for Climate (WDCC) at DKRZ [data set], https://doi.org/10.1594/WDCC/coastDat-1_HAMSOM, 2012.

Hjøllo, S. S., Skogen, M. D., and Svendsen, E.: Exploring currents and heat within the North Sea using a numerical model, J. Marine Syst., 78, 180–192, https://doi.org/10.1016/j.jmarsys.2009.06.001, 2009.

Hobday, A. J., Alexander, L. V., Perkins, S. E., Smale, D. A., Straub, S. C., Oliver, E. C., Benthuysen, J. A., Burrows, M. T., Donat, M. G., Feng, M., Holbrook, N. J., Moore, P. J., Scannell, H. A., Sen Gupta, A., and Wernberg, T.: A hierarchical approach to defining marine heatwaves, Prog. Oceanogr., 141, 227–238, https://doi.org/10.1016/j.pocean.2015.12.014, 2016.

Hövel, L., Brune, S., and Baehr, J.: Decadal Prediction of Marine Heatwaves in MPI-ESM, Geophys. Res. Lett., 49, e2022GL099347, https://doi.org/10.1029/2022GL099347, 2022.

Høyer, J. L. and Karagali, I.: Sea Surface Temperature Climate Data Record for the North Sea and Baltic Sea, J. Climate, 29, 2529–2541, https://doi.org/10.1175/JCLI-D-15-0663.1, 2016.

Høyer, J. L. and She, J.: Optimal interpolation of sea surface temperature for the North Sea and Baltic Sea, J. Marine Syst., 65, 176–189, https://doi.org/10.1016/j.jmarsys.2005.03.008, 2007.

Hu, L.: A Global Assessment of Coastal Marine Heatwaves and Their Relation With Coastal Urban Thermal Changes, Geophys. Res. Lett., 48, e2021GL093260, https://doi.org/10.1029/2021GL093260, 2021.

Huang, B., Liu, C., Banzon, V., Freeman, E., Graham, G., Hankins, B., Smith, T., and Zhang, H.-M.: Improvements of the Daily Optimum Interpolation Sea Surface Temperature (DOISST) Version 2.1, J. Climate, 34, 2923–2939, https://doi.org/10.1175/JCLI-D-20-0166.1, 2021.

Jacobs, Z. L., Jebri, F., Wakelin, S., Strong, J., Popova, E., Srokosz, M., and Loveridge, A.: Marine heatwaves and cold spells in the Northeast Atlantic: what should the UK be prepared for?, Front. Mar. Sci., Volume 11, https://doi.org/10.3389/fmars.2024.1434365, 2024.

Krieger, D., Brune, S., Pieper, P., Weisse, R., and Baehr, J.: Skillful decadal prediction of German Bight storm activity, Nat. Hazards Earth Syst. Sci., 22, 3993–4009, https://doi.org/10.5194/nhess-22-3993-2022, 2022.

Krieger, D., Weisse, R., Baehr, J., and Borchert, L. F.: Machine Learning-Driven Skillful Decadal Predictions of German Bight Storm Surges, Geophys. Res. Lett., 52, e2024GL111558, https://doi.org/10.1029/2024GL111558, 2025.

Lee, T., Fukumori, I., and Tang, B.: Temperature Advection: Internal versus External Processes, J. Phys. Oceanogr., 34, 1936–1944, https://doi.org/10.1175/1520-0485(2004)034<1936:TAIVEP>2.0.CO;2, 2004.

Lellouche, J.-M., Eric, G., Romain, B.-B., Gilles, G., Angélique, M., Marie, D., Clément, B., Mathieu, H., Olivier, L. G., Charly, R., Tony, C., Charles-Emmanuel, T., Florent, G., Giovanni, R., Mounir, B., Yann, D., and Pierre-Yves, L. T.: The Copernicus Global 1/12° Oceanic and Sea Ice GLORYS12 Reanalysis, Front. Earth Sci., 9, https://doi.org/10.3389/feart.2021.698876, 2021.

Lin, Y., Liu, Z., Zhou, F., Meng, Q., and Zhang, W.: Synergistic Impacts of Climate Variabilities on Marine Heatwaves in Shelf Seas, Research Square, PREPRINT (Version 1), https://doi.org/10.21203/rs.3.rs-6503093/v1, 2025.

Locarnini, R. A., Mishonov, A. V., Antonov, J. I., Boyer, T. P., Garcia, H. E., Baranova, O. K., Zweng, M. M., Paver, C. R., Reagan, J. R., Johnson, D. R., Hamilton, M., Seidov, 1948, D., and Levitus, S.: World ocean atlas 2013, Volume 1, Temperature, https://doi.org/10.7289/V55X26VD, 2013.

Madec, G.: NEMO ocean engine, Zenodo, https://doi.org/10.5281/zenodo.3248739, 2016.

Mathis, M., Elizalde, A., Mikolajewicz, U., and Pohlmann, T.: Variability patterns of the general circulation and sea water temperature in the North Sea, Prog. Oceanogr., 135, 91–112, https://doi.org/10.1016/j.pocean.2015.04.009, 2015.

Meyer, E. M., Pohlmann, T., and Weisse, R.: Thermodynamic variability and change in the North Sea (1948–2007) derived from a multidecadal hindcast, J. Marine Syst., 86, 35–44, https://doi.org/10.1016/j.jmarsys.2011.02.001, 2011.

Mohamed, B., Barth, A., and Alvera-Azcárate, A.: Extreme marine heatwaves and cold-spells events in the Southern North Sea: classifications, patterns, and trends, Front. Mar. Sci., 10, https://doi.org/10.3389/fmars.2023.1258117, 2023.

Mohamed, B., Barth, A., Van der Zande, D., and Alvera-Azcárate, A.: Amplified warming and marine heatwaves in the North Sea under a warming climate and their impacts, Ocean Sci., 21, 2505–2525, https://doi.org/10.5194/os-21-2505-2025, 2025.

Okajima, S., Kosaka, Y., Miyasaka, T., and Ito, R.: Unprecedented Marine Heatwave Significantly Exacerbated the Record-Breaking 2023 East Asian Summer Heatwave, AGU Advances, 6, e2025AV001673, https://doi.org/10.1029/2025AV001673, 2025.

Pedregosa, F., Varoquaux, G., Gramfort, A., Michel, V., Thirion, B., Grisel, O., Blondel, M., Prettenhofer, P., Weiss, R., Dubourg, V., Vanderplas, J., Passos, A., Cournapeau, D., Brucher, M., Perrot, M., and Duchesnay, E.: Scikit-learn: Machine Learning in Python, J. Mach. Learn. Res., 12, 2825–2830, 2011.

Pohlmann, T.: Simulating the heat storage in the North Sea with a three-dimensional circulation model, Cont. Shelf Res., 16, 195–213, https://doi.org/10.1016/0278-4343(95)00032-V, 1996.

Rayner, N. A., Parker, D. E., Horton, E. B., Folland, C. K., Alexander, L. V., Rowell, D. P., Kent, E. C., and Kaplan, A.: Global analyses of sea surface temperature, sea ice, and night marine air temperature since the late nineteenth century, J. Geophys. Res.-Atmos., 108, https://doi.org/10.1029/2002JD002670, 2003.

Schulzki, T., Schwarzkopf, F. U., and Biastoch, A.: An Atlantic-wide assessment of marine heatwaves beyond the surface in an eddy-rich ocean model, Ocean Sci., 21, 2481–2504, https://doi.org/10.5194/os-21-2481-2025, 2025.

Schulzki, T., Schwarzkopf, F. U., and Biastoch, A.: High-resolution hindcast simulation of the North Sea in a global ocean – sea-ice model, GEOMAR Helmholtz Centre for Ocean Research Kiel [data set], https://hdl.handle.net/20.500.12085/f2d595cc-10c7-11f1-a464-005056a30ade (last access: 3 February 2026), 2026a.

Schulzki, T., Schwarzkopf, F. U., and Biastoch, A.: The past evolution of marine heatwaves and their drivers in the southern North Sea, GEOMAR Helmholtz Centre for Ocean Research Kiel [data set], https://hdl.handle.net/20.500.12085/6dd5ffce-10c7-11f1-a1b6-005056a30ade (last access: 3 February 2026), 2026b.

Semmouri, I., De Schamphelaere, K. A., Mortelmans, J., Mees, J., Asselman, J., and Janssen, C. R.: Decadal decline of dominant copepod species in the North Sea is associated with ocean warming: Importance of marine heatwaves, Mar. Pollut. Bull., 193, 115159, https://doi.org/10.1016/j.marpolbul.2023.115159, 2023.

Smale, D. A., Wernberg, T., Oliver, E. C. J., Thomsen, M., Harvey, B. P., Straub, S. C., Burrows, M. T., Alexander, L. V., Benthuysen, J. A., Donat, M. G., Feng, M., Hobday, A. J., Holbrook, N. J., Perkins-Kirkpatrick, S. E., Scannell, H. A., Sen Gupta, A., Payne, B. L., and Moore, P. J.: Marine heatwaves threaten global biodiversity and the provision of ecosystem services, Nat. Clim. Change, 9, 306–312, https://doi.org/10.1038/s41558-019-0412-1, 2019.

Smith, K. E., Burrows, M. T., Hobday, A. J., King, N. G., Moore, P. J., Sen Gupta, A., Thomsen, M. S., Wernberg, T., and Smale, D. A.: Biological Impacts of Marine Heatwaves, Annu. Rev. Mar. Sci., 15, 119–145, https://doi.org/10.1146/annurev-marine-032122-121437, 2023.

Smith, K. E., Sen Gupta, A., Amaya, D., Benthuysen, J. A., Burrows, M. T., Capotondi, A., Filbee-Dexter, K., Frölicher, T. L., Hobday, A. J., Holbrook, N. J., Malan, N., Moore, P. J., Oliver, E. C., Richaud, B., Salcedo-Castro, J., Smale, D. A., Thomsen, M., and Wernberg, T.: Baseline matters: Challenges and implications of different marine heatwave baselines, Prog. Oceanogr., 231, 103404, https://doi.org/10.1016/j.pocean.2024.103404, 2025.

Taylor, A. and Stephens, J.: Seasonal and year-to-year changes in the temperatures of the English Channel and the Southern North Sea, 1961–1976: a budget, Oceanol. Acta, 6, 63–72, 1983.

Thomson, R. E. and Emery, W. J.: Chapter 3 – Statistical Methods and Error Handling, in: Data Analysis Methods in Physical Oceanography (Third Edition), edited by: Thomson, R. E. and Emery, W. J., Elsevier, Boston, ISBN 978-0-12-387782-6, 219–311, https://doi.org/10.1016/B978-0-12-387782-6.00003-X, 2014.

Tsujino, H., Urakawa, S., Nakano, H., Small, R. J., Kim, W. M., Yeager, S. G., Danabasoglu, G., Suzuki, T., Bamber, J. L., Bentsen, M., Böning, C. W., Bozec, A., Chassignet, E. P., Curchitser, E., Boeira Dias, F., Durack, P. J., Griffies, S. M., Harada, Y., Ilicak, M., Josey, S. A., Kobayashi, C., Kobayashi, S., Komuro, Y., Large, W. G., Le Sommer, J., Marsland, S. J., Masina, S., Scheinert, M., Tomita, H., Valdivieso, M., and Yamazaki, D.: JRA-55 based surface dataset for driving ocean–sea-ice models (JRA55-do), Ocean Model., 130, 79–139, https://doi.org/10.1016/j.ocemod.2018.07.002, 2018.

Tsujino, H., Urakawa, L. S., Griffies, S. M., Danabasoglu, G., Adcroft, A. J., Amaral, A. E., Arsouze, T., Bentsen, M., Bernardello, R., Böning, C. W., Bozec, A., Chassignet, E. P., Danilov, S., Dussin, R., Exarchou, E., Fogli, P. G., Fox-Kemper, B., Guo, C., Ilicak, M., Iovino, D., Kim, W. M., Koldunov, N., Lapin, V., Li, Y., Lin, P., Lindsay, K., Liu, H., Long, M. C., Komuro, Y., Marsland, S. J., Masina, S., Nummelin, A., Rieck, J. K., Ruprich-Robert, Y., Scheinert, M., Sicardi, V., Sidorenko, D., Suzuki, T., Tatebe, H., Wang, Q., Yeager, S. G., and Yu, Z.: Evaluation of global ocean–sea-ice model simulations based on the experimental protocols of the Ocean Model Intercomparison Project phase 2 (OMIP-2), Geosci. Model Dev., 13, 3643–3708, https://doi.org/10.5194/gmd-13-3643-2020, 2020.

van Leeuwen, S., Tett, P., Mills, D., and van der Molen, J.: Stratified and nonstratified areas in the North Sea: Long-term variability and biological and policy implications, J. Geophys. Res.-Oceans, 120, 4670–4686, https://doi.org/10.1002/2014JC010485, 2015.

Waters, J., Lea, D. J., Martin, M. J., Mirouze, I., Weaver, A., and While, J.: Implementing a variational data assimilation system in an operational 1/4 degree global ocean model, Q. J. Roy. Meteor. Soc., 141, 333–349, https://doi.org/10.1002/qj.2388, 2015.

Wernberg, T., Smale, D. A., Tuya, F., Thomsen, M. S., Langlois, T. J., de Bettignies, T., Bennett, S., and Rousseaux, C. S.: An extreme climatic event alters marine ecosystem structure in a global biodiversity hotspot, Nat. Clim. Change, 3, 78–82, https://doi.org/10.1038/nclimate1627, 2013.

Zhang, X., Zhao, N., Han, Z., and Dai, Z.: Large spread in marine heatwave assessments for Asia and the Indo-Pacific between sea-surface-temperature products, Commun. Earth Environ., 5, 195, https://doi.org/10.1038/s43247-024-01369-9, 2024.

Zhang, Y., Feng, M., Du, Y., Phillips, H. E., Bindoff, N. L., and McPhaden, M. J.: Strengthened Indonesian Throughflow Drives Decadal Warming in the Southern Indian Ocean, Geophys. Res. Lett., 45, 6167–6175, https://doi.org/10.1029/2018GL078265, 2018.

Zweng, M. M., Reagan, J. R., Antonov, J. I., Locarnini, R. A., Mishonov, A. V., Boyer, T. P., Garcia, H. E., Baranova, O. K., Johnson, D. R., Seidov, D., Biddle, M. M., and Levitus, S.: World ocean atlas 2013, Volume 2, Salinity, https://doi.org/10.7289/V5251G4D, 2013.